ELSEVIER

www.elsevier.nl/locate/jorganchem

Journal of Organometallic Chemistry 591 (1999) 45–62

Journal of Organometallic Chemistry

The metal–carbon multiple bond in iron(I)– and iron(II)–dibenzotetramethyltetra[14]azaannulene: carbene, carbonyl, and isocyanide derivatives

Alain Klose [a], Joëlle Hesschenbrouck [a], Euro Solari [a], Mario Latronico [a,1], Carlo Floriani [a,*], Nazzareno Re [b], Angiola Chiesi-Villa [c], Corrado Rizzoli [c]

[a] *Institut de Chimie Minérale et Analytique, BCH, Université de Lausanne, CH-1015 Lausanne, Switzerland*
[b] *Facoltà di Farmacia, Università degli Studi 'G. D'Annunzio', I-66100 Chieti, Italy*
[c] *Dipartimento di Chimica, Università di Parma, I-43100 Parma, Italy*

Received 25 May 1999; accepted 13 June 1999

Abstract

The two parent compounds used for studying the iron–carbon multiple bond interactions are [Fe(tmtaa)] (**1**), and [Fe(tmtaa)Na(THF)$_3$] (**2**) [tmtaa≡dibenzotetramethyltetraaza[14]annulene dianion], the latter being obtained by reduction of **1**. The reaction of **1** with CO led to the corresponding monocarbonyl derivative [Fe(tmtaa)(CO)(L)] [L = THF, **3**; L = Py, **4**], while the reaction with RNC allowed us to isolate mono-isocyanide [Fe(tmtaa)(*o*-Me$_3$Si–C$_6$H$_4$NC)(THF)] (**5**), [Fe(tmtaa)(^{n}BuNC)(THF)] (**6**), and bis-isocyanide [Fe(tmtaa)(^{t}BuNC)$_2$] (**7**) derivatives. Reduction of **6** with sodium metal or the reaction of **1** with NaCN led to a monocyano derivative bridged into a dimeric form by sodium cations in [{Fe(tmtaa)(CN)}$_2$(μ-NaL$_n$)$_2$] [L = THF, $n = 3$, **8a**; L = DME, $n = 2$, **8b**], while the reaction of **1** with ^{n}Bu$_4$N$^+$CN$^-$ led to the monomeric form [Fe(tmtaa)(CN)]$^-$(^{n}Bu$_4$N)$^+$ (**9**). A detailed magnetic analysis of **1**–**10**, the last one being the bis-pyridine derivative [Fe(tmtaa)(Py)$_2$] (**10**) showed a variety of low and intermediate spin states, and spin crossovers (with a minor role played by high spin states) as a function of the axial ligands. A remarkable difference was observed with the analogous porphyrin derivatives. The d^7 iron(I) derivative **2** occurs in tight ion-pair form, both iron and sodium being bonded to the tmtaa ligand. The reaction of **2** with carbon monoxide led to a monocarbonyl derivative bridged in a dimeric form by sodium cations bonded to the oxygen atoms in [{Fe(tmtaa)}$_2${μ-CONa(THF)$_2$}$_2$] (**11**). Both **2** and **11** showed a spin conversion between $S = 1/2$ and $S = 3/2$, with a small antiferromagnetic coupling in the latter case, due to the dimeric form. The reaction of **1** with diazoalkane RR′CN$_2$ led to the corresponding low-spin diamagnetic carbene derivatives [Fe(tmtaa)(CRR′)] [R = R′ = Ph, **12**; R = Ph, R′ = H, **13**], the first one being by far more thermally stable, while the second one decomposes at room temperature to **1** and a mixture of *cis* and *trans*-stilbene. Both react with O$_2$ giving Ph$_2$CO and PhCHO and the μ-oxo dimer [{Fe(tmtaa)}(μ-O)] (**14**). The proposed structures are supported by the X-ray analyses on complexes **2**, **8b**, **9**, **11b** and **12**.

Keywords: Metalla-macrocycle; Iron carbene; Iron–carbon monoxide; Iron macrocycle redox

1. Introduction

Macrocycles are increasingly considered as ancillary ligands in organometallic chemistry [1–7]. This trend has been developed particularly in recent years for early transition metals. In the case of middle transition metals, however, the metal–carbon functionalities have been essentially considered for their relationship with biologically occurring systems, namely vitamin B$_{12}$ in the case of cobalt [8] and the cytochrome P450 in the case of iron [9]. The macrocycle par excellence used in such a context has been the porphyrin skeleton, with important contributions in Ru [10a] and Rh [10b] chemistry. A number of other model ligands, however, have been considered and among them particularly the tetradentate Schiff bases [6] and the dibenzo-

* Corresponding author. Fax: +41-21-6923905.
E-mail address: carlo.floriani@icma.unil.ch (C. Floriani)
[1] Present address: Dipartimento di Ingegneria e Fisica dell'Ambiente, Università della Basilicata, via della Tecnica 3, I-85100 Potenza, Italy.

0022-328X/99/$ - see front matter
PII: S0022-328X(99)00354-X

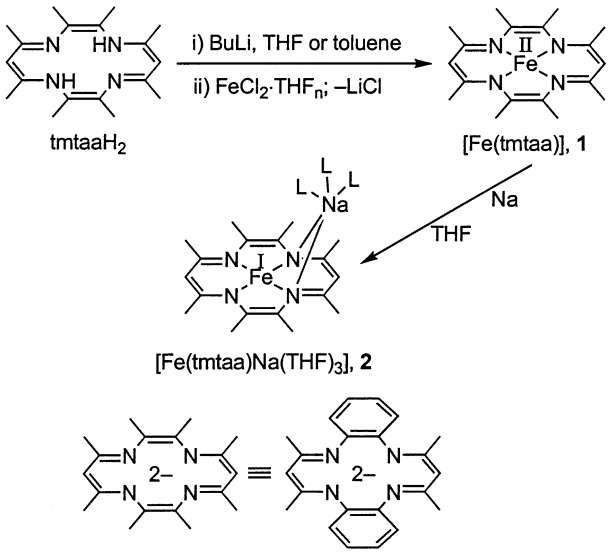

Scheme 1.

tetramethyltetraaza[14]annulene [2]. In the latter case, some fundamental work has been developed by the groups of Goedken [11] and Cotton [12]. The present report deals with the synthesis and the properties of iron(II) and iron(I)–dibenzotetramethyltetraaza-[14]annulene [tmtaa] complexes, containing a multiple bond to carbon ligands, namely CO, RNC, carbene, and cyanides. The nature of some starting iron(II)–tmtaa complexes has been elucidated by Goedken and co-workers [11], though large-scale and improved syntheses are reported here. Particularly remarkable are: (i) the stabilization of the iron–carbene multiple bond functionalities; and (ii) the magnetic properties associated both to the iron(I) and iron(II) derivatives. Some results have been published in preliminary communications [13,14].

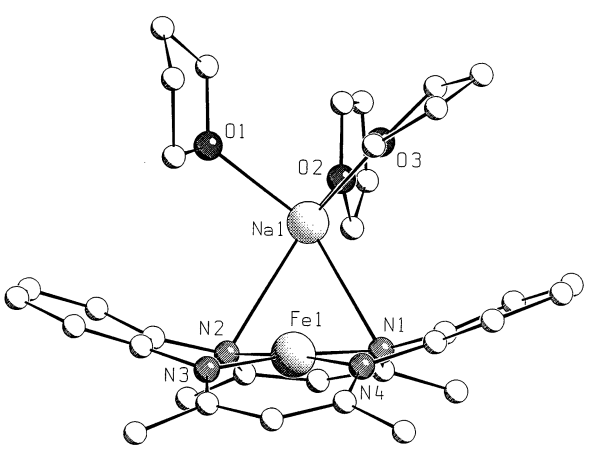

Fig. 1. SCHAKAL view of molecule A in complex **2**.

2. Results and discussion

2.1. Synthesis of iron(II)– and iron(I)–tmtaa derivatives

Two different approaches for synthesizing complex [Fe(tmtaa)] **1** are known [11a,h]. Our method, which is reproducible on a 20 g scale, involved reacting $[FeCl_2(THF)_{1.5}]$ with the deprotonated tmtaa ligand (Scheme 1) [2d].

Complex **1** formed as a poorly soluble crystalline solid in THF. This feature made its isolation easy since the related inorganic salt is very soluble in the solvent. An NMR spectrum could only be obtained in pyridine-d_5 and showed broad signals due to the paramagnetic behavior of the molecule (see below). Elemental analysis suggested the inclusion of a THF molecule. The X-ray analysis has already been reported by Goedken et al. [11h] and shows that the ligand has the familiar saddle shape conformation, with iron displaced slightly from the N_4 plane (0.114 Å). The axial positions are not occupied suggesting their potential for coordinating other substrates.

When **1** was reduced with exactly one equivalent of sodium in THF, complex **2** formed in high yield (Scheme 1). The magnetic analysis of this very air-sensitive complex is reported in the following section. The X-ray analysis is given in Fig. 1 and shows the ion pair structure of **2**, the molecule B between the two independent ones being only considered. The ion pairing phenomenon has already been observed in the reduced form of metal Schiff base complexes [15] and in porphyrin derivatives [16].

Crystallographic data and details associated with data collection are given in Table 1. Selected bond distances and angles for all complexes are quoted in Table 2. Relevant conformational parameters within the [Fe(tmtaa)] moieties are given in Table 3. The labeling scheme adopted for the tmtaa ligand is depicted below.

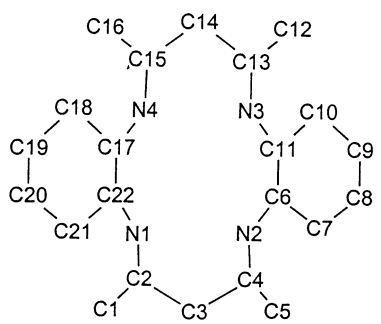

Both iron and sodium cations are bonded to the macrocycle. The distance of the iron to the N_4 coordination plane of 0.092(1) Å is indicative of a change in the oxidation state and supports a d^7 configuration.

Table 1
Experimental data for the X-ray diffraction studies on crystalline complexes **2**, **8b**, **9**, **11b** and **12**

Complex	**2**	**8b**	**9**	**11b**	**12**
Formula	$C_{34}H_{46}FeN_4NaO_3$	$C_{62}H_{84}Fe_2N_{10}Na_2O_8 \cdot C_4H_{10}O_2$	$C_{23}H_{22}FeN_5 \cdot C_{16}H_{36}N \cdot 2C_4H_8O$	$C_{62}H_{84}Fe_2N_8Na_2O_{10} \cdot 5C_6H_6$	$C_{35}H_{32}FeN_4 \cdot C_7H_8$
a (Å)	10.441(2)	11.484(2)	12.256(2)	13.879(2)	11.670(3)
b (Å)	17.648(4)	15.037(3)	22.060(4)	15.549(2)	13.593(4)
c (Å)	34.799(7)	11.360(2)	17.302(2)	21.326(3)	11.234(3)
α (°)	90	106.43(2)	90	99.07(2)	106.72(2)
β (°)	92.51(3)	101.96(1)	107.87(2)	98.80(2)	96.21(2)
γ (°)	90	106.38(1)	90	98.02(2)	77.62(2)
V (Å^3)	6406(2)	1715.2(6)	4452.2(13)	4427.6(12)	1665.0(8)
Z	8	1	4	2	2
Formula weight	637.6	1345.2	811.0	1649.6	656.7
Space group	$P2_1/c$ (no. 14)	$P\bar{1}$ (no. 2)	$P2_1/n$ (no. 14)	$P\bar{1}$ (no. 2)	$P\bar{1}$ (no. 2)
T (°C)	22	−140	−140	22	−140
λ (Å)	0.71069	0.71069	0.71069	0.71069	0.71069
$\rho_{calc.}$ (g cm^{-3})	1.322	1.302	1.210	1.237	1.310
μ (cm^{-1})	5.21	4.94	3.79	3.94	4.86
Transmission coefficients	0.758–1.000	0.674–1.000	0.647–1.000	0.921–1.000	0.562–1.000
R [a]	0.082	0.073	0.055	0.086	0.059
wR_2 [b]	0.166	0.203	0.164	0.249	0.163
Goodness-of-fit	1.208	1.066	0.988	1.118	1.021
N-observed [c]	5897	2793	4809	8549	4428
N-independent [d]	11168	3295	9915	17976	5831
N-refinement [e]	5897	3082	8286	10999	5293
Variables	776	392	505	979	424

[a] Calculated on the unique observed data having $I = 2\sigma(I)$ for **8b**, **9**, **11b**, **12** and $I = 3\sigma(I)$ for **2**.
[b] Calculated on the unique data with $I = 0$ for **8b**, **9**, **11b**, **12** and with $I = 3\sigma(I)$ for **2**.
[c] N-observed is the total number of the independent reflections having $I = 2\sigma(I)$ for **8b**, **9**, **11b**, **12** and $I = 3\sigma(I)$ for **2**.
[d] N-independent is the number of independent reflections.
[e] N-refinement is the number of reflection used in the refinement having $I = 0$ for **8b**, **9**, **11b**, **12** and $I = 3\sigma(I)$ for **2**.

Table 2
Selected bond lengths (Å) and angles (°) for complexes **2**, **8b**, **9**, **11b** and **12**

	2		**8b**	**9**	**11b**		**12**
	Mol A	Mol B			Mol A	Mol B	
Bond lengths							
Fe–N(1)	1.898(5)	1.886(6)	1.928(5)	2.061(2)	1.986(4)	2.053(4)	1.921(3)
Fe–N(2)	1.895(5)	1.894(5)	1.924(5)	2.056(3)	2.004(4)	2.044(4)	1.926(2)
Fe–N(3)	1.914(6)	1.904(5)	1.920(6)	2.050(2)	1.994(4)	2.045(5)	1.911(3)
Fe–N(4)	1.912(5)	1.920(6)	1.912(6)	2.057(4)	1.998(4)	2.043(4)	1.920(2)
Fe–C(23)			1.844(8)	2.084(4)	1.752(5)	1.758(5)	1.794(3)
N(1)–C(2)	1.375(9)	1.360(10)	1.349(8)	1.327(4)	1.322(7)	1.328(8)	1.333(4)
N(1)–C(22)	1.396(9)	1.409(9)	1.401(9)	1.421(5)	1.410(7)	1.405(7)	1.418(4)
N(2)–C(4)	1.356(9)	1.342(9)	1.345(9)	1.338(4)	1.326(8)	1.322(8)	1.321(5)
N(2)–C(6)	1.419(9)	1.431(9)	1.404(10)	1.410(4)	1.414(6)	1.408(7)	1.418(5)
N(3)–C(11)	1.435(9)	1.407(9)	1.413(9)	1.429(5)	1.401(8)	1.414(6)	1.422(4)
N(3)–C(13)	1.341(9)	1.364(9)	1.355(7)	1.329(5)	1.325(6)	1.330(6)	1.327(5)
N(4)–C(15)	1.343(9)	1.325(10)	1.367(7)	1.324(4)	1.337(6)	1.318(8)	1.333(5)
N(4)–C(17)	1.416(9)	1.425(10)	1.389(9)	1.421(4)	1.417(6)	1.402(8)	1.409(5)
X–C(23) [a]			1.167(10)	1.160(6)	1.202(7)	1.196(7)	
C(23)–C(31)							1.487(7)
C(23)–C(41)							1.472(4)
Bond angles							
Fe–C(23)–X [a]			179.6(6)	179.3(4)	177.8(4)	178.2(4)	
Fe–C(23)–C(41)							122.6(2)
Fe–C(23)–C(31)							121.7(2)
C(31)–C(23)–C(41)							115.7(3)

[a] X should be read N(5) for **8b**, **9** and O(1) for **11b**.

Table 3
Comparison of relevant conformational parameters within Fe(tmtaa) moiety for complexes **2**, **8b**, **9**, **11b** and **12**

	2		**8b**	**9**	**11b**		**12**
	Mol A	Mol B			Mol A	Mol B	
(a) Distances (Å) *of atoms from the N_4 mean plane*							
N(1)	0.003(7)	0.018(7)	−0.004(5)	0.014(2)	0.032(5)	0.003(4)	−0.057(2)
N(2)	−0.003(7)	−0.018(7)	0.005(5)	−0.014(2)	−0.031(5)	−0.003(4)	0.057(2)
N(3)	0.003(7)	0.018(7)	−0.008(6)	0.014(2)	0.031(5)	0.003(4)	−0.057(2)
N(4)	−0.003(7)	−0.018(7)	0.005(5)	−0.014(2)	−0.025(4)	−0.003(4)	0.057(2)
Fe(1)	0.092(1)	0.093(1)	0.266(1)	0.610(1)	0.553(2)	0.655(2)	0.335(1)
(b) Dihedral angles (°) *between significant planes*							
$N_4 \wedge N(1)C_3N(2)$	158.7(3)	159.2(3)	154.7(2)	146.2(1)	149.9(1)	146.5(2)	153.1(1)
$N_4 \wedge N(3)C_3N(4)$	158.1(2)	158.6(2)	154.7(2)	144.6(1)	148.0(2)	145.3(2)	154.7(1)
$N_4 \wedge N(1)C_6N(4)$	161.6(2)	160.1(2)	160.3(1)	167.0(1)	163.5(1)	162.3(1)	155.2(1)
$N_4 \wedge N(2)C_6N(3)$	159.7(2)	160.4(2)	160.4(2)	166.5(1)	161.9(1)	162.2(1)	154.2(1)
$N(1)C_3N(2) \wedge N(3)C_3N(4)$	136.8(3)	137.7(3)	129.4(2)	110.8(1)	117.9(2)	111.8(2)	127.8(1)
$N(1)C_6N(4) \wedge N(2)C_6N(3)$	141.2(1)	140.6(1)	140.7(1)	153.5(1)	145.4(1)	144.6(1)	130.1(1)
C(6)···C(11) ∧ C(17)···C(22)	138.2(2)	136.8(2)	136.1(2)	149.5(1)	140.9(2)	139.1(2)	123.1(1)

The same value was obtained for the isoelectronic complex [Co(tmtaa)] [11a]. One other factor to consider is the average Fe–N bond length. This distance decreases with respect to the metal center–N_4 plane distance or as its d^n configuration increases, varying from 2.054 Å for [Fe(tmtaa)$_2$O]·MeCN [11o] to 2.002 Å for [Fe(tmtaa)Cl]·MeCN [11a], to 1.918 Å in **1** [11h] and 1.904(5) Å in **2**. It is worth noting that, at variance with the iron porphyrin anion $[Fe(TPP)]^-$ [16a], no significant change at the bond distance pattern in the tetraaza macrocycle ligand is observed. This supports the proposed $[Fe^{I}(tmtaa)]^-$ iron(I) formulation over the alternative $[Fe^{II}(tmtaa^{\bullet})]^-$ iron(II)-π radical anion, which is instead suggested in the porphyrin analogue [16a], though a later study was more in favor of the iron(I)-d^7 formulation for $[Fe(TPP)]^-$ [16c]. A more significant difference is observed between iron(II) and iron(I) complexes. The tmtaa ligand shows the usual saddle shape conformation (Table 3). The sodium cation binds to the tmtaa ligand interacting with the N(1) and N(2) nitrogen atoms at rather long distances (Na(1)–N(1), 2.784(7) [2.747(8)] Å; Na(1)–N(2), 2.810(8) [2.845(7)] Å). Complex **2** is bifunctional and contains, in close proximity, two different reactive metal sites, namely iron and sodium. The nucleophilic iron shows very interesting reactivity with small molecules and organic functionalities (see below).

2.2. Reactivity of [Fe(tmtaa)] (*1*), with CO, isocyanides, and cyanides

Coordination to **1** of strong field ligands, such as CO, cyanides, and isonitriles, gave complexes that could be characterized with NMR spectroscopy, although their magnetic measurement do not suggest a diamagnetic behavior. These complexes (see Scheme 1) were easily accessible, and were all isolated in crystalline form and in good yield. A general overview of the reactions is presented in Scheme 2.

The reaction of **1** with CO readily formed monocarbonyl complexes either in the presence or the absence of other axial ligand like pyridine or THF. Complex **3** was obtained from the reaction of **1** with CO in THF. The strong binding of CO is indicated by the characteristic IR band displaced from 2155 cm^{-1} for free CO to 1913 cm^{-1} for **3**. This indicates a relevant back-donation process. The reactivity of CO was also observed by its ability to displace one coordinated pyridine in the complex $[Fe(tmtaa)(Py)_2]$ (**10**) formed in situ. The re-

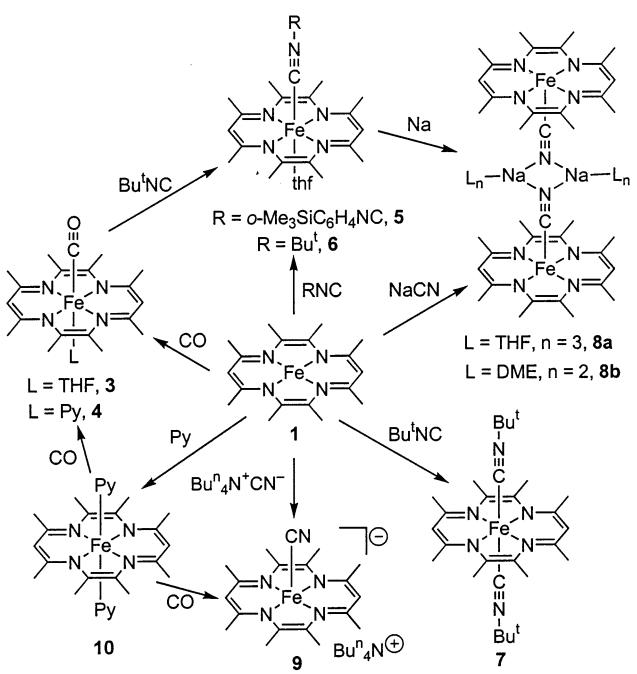

Scheme 2.

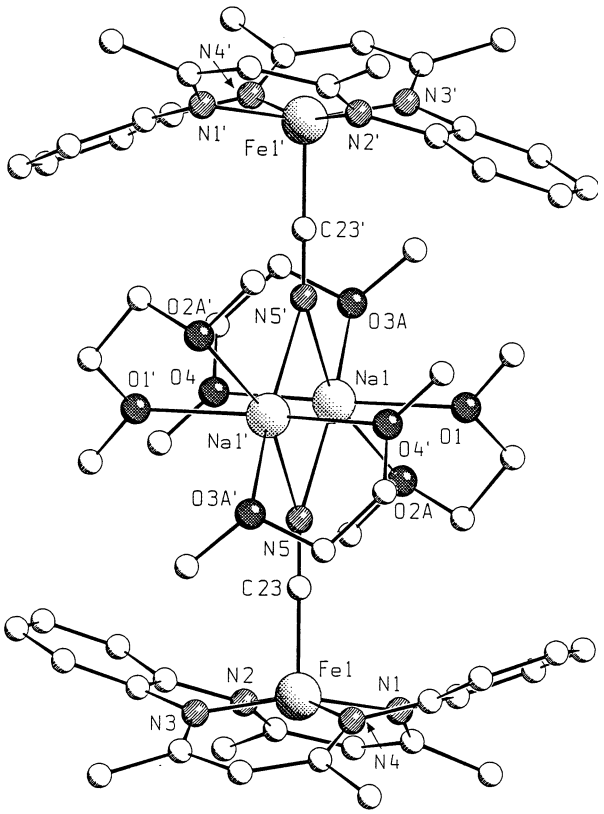

Fig. 2. SCHAKAL view of complex **8b**. Disorder affecting the DME molecules has been omitted for clarity. A prime denotes a transformation of $-x, -1-y, -z$.

sulting compound **4** shows a slight variation in its IR spectrum with the CO band centered at 1927 cm^{-1}. ^{1}H-NMR spectra were obtained for both complexes despite the paramagnetic behavior of **3** ($\mu_{eff.} = 3.10\mu_B$ at 298 K) (see below). These two spectra were recorded in pyridine-d_5 and are the same except that **3** includes the THF peaks. Each set of tmtaa signals also shows similar weak resonances, which do not correspond to **10**. This can be explained by the formation of a very small amount of [Fe(tmtaa)$(CO)_2$], although rarely observed because of the high lability of the second coordinated CO [17], or by the possibility of a spin state equilibrium, which will give rise to a paramagnetic contribution. Complexes [Fe(tmtaa)(CO)], [Fe(tmtaa)(CO)(Py)] (**4**) and [Fe(tmtaa)$(CO)(N_2H_4)$] have been reported by Goedken et al. [11h]. However, they have not been obtained from the carbonylation of **1**, except during the in situ synthesis of **1** under a carbon monoxide atmosphere. In addition, no detail is given concerning the magnetic properties of such compounds.

In contrast to CO, the stronger σ-donor isonitriles can selectively give mono- or bis-coordinated complexes. When **1** was reacted with one equivalent of RNC in THF, the resulting microcrystalline products of poor solubility **5** (R = *o*-$Me_3SiC_6H_4NC$) and **6** (R = ^{t}BuNC) were isolated. Characteristic isonitrile IR bands were observed at 2076 cm^{-1}, **5**, and 1989 cm^{-1}, **6**. The comparison with the free isonitriles (2123 cm^{-1}, *o*-$Me_3SiC_6H_4NC$; 2134 cm^{-1}, ^{t}BuNC) suggests a strong back-donation. The ^{1}H-NMR spectra of **5** does not show any unusual behavior, in contrast to **6**, which gave additional peaks of low integration similar to the carbonyl compound **3**. These signals do not belong to the bis-isonitrile complex **7** or to **1**. The explanation of a paramagnetic contribution can similarly be suggested, although in this case the compound is essentially diamagnetic with a little residual paramagnetism, probably due to paramagnetic impurities or temperature-independent paramagnetism (TIP). A quite common method was used to form complex **6** and involves the displacement of the carbonyl ligand in **3** by ^{t}BuNC.

A crystalline product of better solubility was obtained when **1** was reacted with two equivalents of ^{t}BuNC. As a result of a second coordination, [Fe(tmtaa)$(^t$BuNC$)_2$] (**7**) showed an IR band shifted to 2089 cm^{-1}. The ^{1}H-NMR spectrum confirms the presence of two ^{t}Bu groups. This spectrum does not show any unusual behavior, except for the broadness of the signals. This may be a consequence of the paramagnetic behavior of the molecule ($\mu_{eff.} = 2.55\mu_B$ at 298 K). The prediction of whether the configuration is *cis* or *trans* can be answered by the iron out-of-plane distance, the electron rich metals being almost in the N_4-plane and they favor a *trans* arrangement [2d]. The IR spectrum with a single C≡N band confirms such an assignment. The reduction of **6** with Na metal in THF is a slow reaction leading to **8a**. Recrystallization of **8a** in DME gave crystals suitable for an X-ray analysis, which confirmed the formation of the cyanide complex **8b** (Fig. 2). In light of this structure, a straightforward synthesis was tested by reacting **1** with sodium cyanide. Because of the poor solubility of NaCN in the organic solvent, a slow reaction was observed under reflux conditions in THF. The analytical and spectroscopic data were in agreement with the cyanide complex **8a**.

The molecular structure of **8b** is given in Fig. 2 and consists of centrosymmetric dimers. Each monomeric unit is bridged to the other through sodium atoms, which are each surrounded by two DME molecules in an octahedral arrangement. The Fe(1)–C(23) distance (1.853(8) Å) is slightly shorter than for other iron(II) complexes (see $[Na_4Fe(CN)_6]$: 1.909 Å (average value) [18]; $[H_4Fe(CN)_6]$: 1.890 Å [19]; $[Na_2Fe(CN)_5NO]$: 1.913 Å) [20]. In contrast the C(23)–N(5) distance of 1.167(10) Å in **8b** is longer (see $[Na_4Fe(CN)_6]$: 1.163 Å; $[H_4Fe(CN)_6]$: 1.149 Å; $[Na_2Fe(CN)_5NO]$: 1.15 Å). This is a result of the higher electronic density of **8** and its stronger back-donation to the cyanide ligand. The out-of-plane distance of the iron from the N_4-plane is 0.266(1) Å and is in agreement with a d^6 configuration. The tmtaa ligand, which shows the usual saddle shape conformation, has structural parameters quite close to those reported for the other iron complexes (Tables 2 and 3).

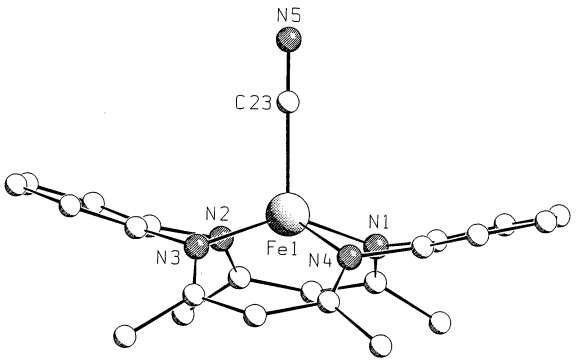

Fig. 3. SCHAKAL view of the anion in complex **9**.

The peculiar magnetic properties of **8a** prompted us to prove if they were essentially associated to the dimeric nature of the complex. In this light, we synthesized the mononuclear cyanide complex **9**, according to the reaction in Scheme 1. Complex **9** displays a C≡N stretching band at 2089 cm^{-1} and magnetic properties different from those of the dimer **8a** (see below).

The structure of **9** consists of discrete $[Fe(tmtaa)(CN)]^-$ anions (Fig. 3), $[N^nBu_4]^+$ cations and THF solvent molecules of crystallization in the stoichiometric molar ratio of 1:1:2. Iron exhibits an almost regular tetragonal pyramidal coordination, the base being defined by the four nitrogen atoms from the N_4 core and the apex by the C(23) carbon atom from the cyanide ligand. The N_4 core is nearly planar, the metal being displaced by 0.610(1) Å (Table 3). The Fe–C(23) vector is nearly perpendicular to the N_4 core, the dihedral angle it forms with the normal to the N_4 mean plane being 2.7(1)°. The Fe–N bond distances are not significantly different from each other (mean value 2.056(3) Å) and are remarkably longer than those observed in **8b**, in agreement with the increased out-of-plane distance of the metal from the N_4. The saddle-shape conformation of the tmtaa ligand differs from those observed in the previous complexes mainly in the mutual orientation of the opposite NC_3N systems, which are pushed toward the cavity to form a dihedral angle of 110.8(1)° versus 136.8(3) [137.7(3)]° and 129.4(2)° in **2** and **8b**, respectively (Table 3). The Fe–C(23) distance (2.084(4) Å) is also remarkably longer than those observed in **8b**. The remarkable differences observed between the structural parameters of **8** and **9**, along with the moving of the C≡N stretching vibration from 2089 cm^{-1} in **9** to 1987 cm^{-1} in **8a**, are due to the different spin states occurring for the monomeric and dimeric species (see below).

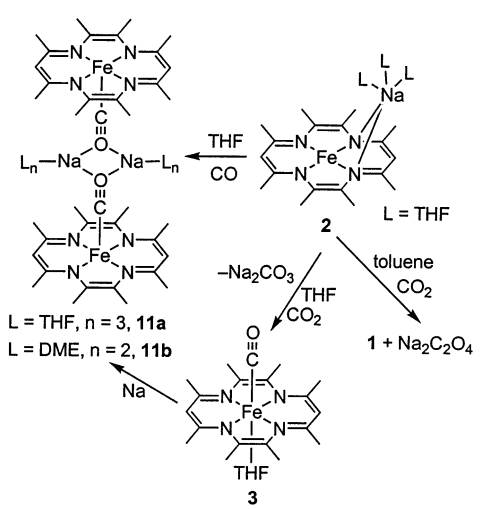

Scheme 3.

2.3. Reactivity of [Fe(tmtaa)Na(THF)$_3$] (2), with carbon monoxide and carbon dioxide

2.3.1. Reaction with CO

There has been considerable interest in the coordination of carbon monoxide to iron and cobalt surrounded by a macrocyclic ligand [11h,21]. In contrast, its reactivity toward transition metal organic anions has received very limited attention, probably due to the fact that their isolation is difficult. Few examples have been reported and these generally involved normal coordination of CO [22]. An exception is seen with [Co(salen)Na], which in the first step of the reaction formed [Co(salen)(CO)Na], and then decomposed to other products [23a,b]. Another remarkable example is the carbonylation of $[Fe^I(TPP)]^-$ carried out in situ and analyzed with spectroscopic and electrochemical tools, though isolation of any CO derivative has not been mentioned [23c]. A rapid reaction was observed when **2** was reacted with CO in chilled (-30°C) THF. The resulting product was very air sensitive. The CO IR band is shifted from 1913 cm^{-1} in **3** to 1736 cm^{-1} in **11**, thus suggesting that coordination had occurred on a Fe(I) center. The remarkable back-donation from Fe(I) (Scheme 3) is coupled with the formation of an iron–carbon multiple bond. Such a decrease in the CO stretching frequency is a further proof of the iron oxidation state (I) in the $[Fe(tmtaa)]^-$ anion, and it should be compared with that at much higher frequency in $[Fe(TPP)(CO)]^-$ (1931 cm^{-1}) [23c]. The high back-donation from iron(I) to carbon monoxide makes the oxygen electron rich, thus suitable for binding the Lewis acid Na^+. This is particularly relevant in the context of the so-called bifunctional activation of carbon monoxide by a simultaneous interaction with an electron-rich and an electron-poor center. In addition, as recently singled out in the reactivity and structural study of $Li_3[Co(CN)_5]$ [24], the alkali cation interacting with the CN^- ligand can be used for tuning the electron density at the transition metal center.

The structure of **11** is displayed in Fig. 4. The dimers crystallize with benzene solvent molecules in a stoichio-

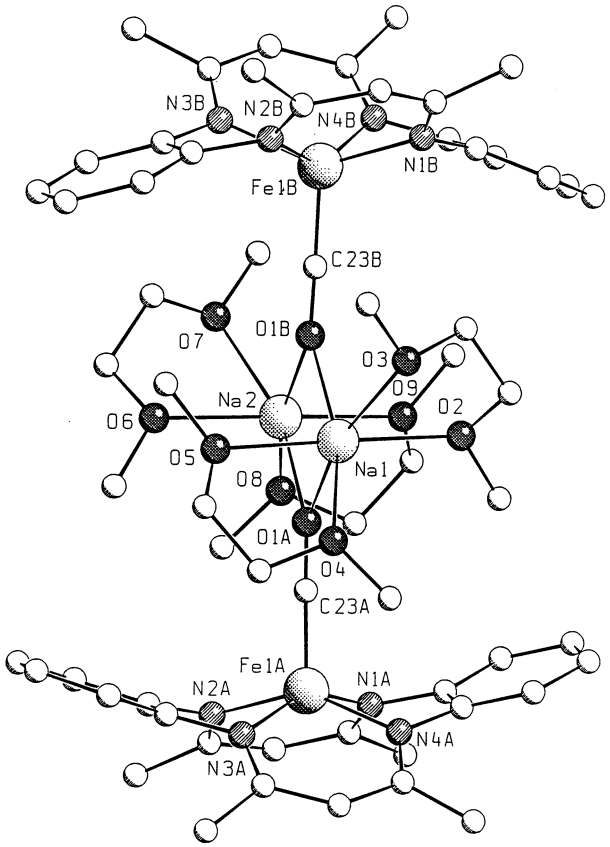

Fig. 4. SCHAKAL view of complex **11b**.

metric molar ratio of 1:5. The two independent tmtaa ligands, for which the labeling shown in Chart 1 has been applied, are referred to as molecule A and B, respectively. Values referring to molecule B will be hereafter given in square brackets. The coordination environment of iron is a distorted tetragonal pyramid, with the metal displaced by 0.553(2) Å [0.655(2) Å] from the N_4 mean plane (Table 3). The Fe–C(23) vector forms a dihedral angle of 1.9(2) [1.6(2)]° with the normal to the N_4 mean plane. The Fe–C(23) bond distance (1.752(5) [1.758(5)] Å) falls in the lower end of values usually observed for Fe–CO (terminal CO) fragments. Coordination around each sodium cation is completed to distorted octahedral through the oxygen atoms from two DME molecules. The magnetic properties of **11** have been analyzed as reported in the following section.

2.3.2. Reaction with CO_2

The general strategies for fixing and subsequently activating CO_2 involved the use of highly basic metals and the utilization of bifunctional systems which contain in their structure the metal in a low oxidation state (basic center) along with an acidic center [25]. A number of metal carbonate complexes were formed on reaction with CO_2. This can be explained by a reductive disproportionation mechanism [25]. A second transformation was also observed and is the deoxygenation process, which liberates CO and forms metal-oxo species [25]. The reaction of **2** with CO_2 is solvent dependent (Scheme 3). When **2** was reacted with CO_2 in THF, two products were detected. The IR spectrum showed clearly **3** having a sharp CO band at 1913 cm^{-1}. The ^{1}H-NMR, however, showed the 1:1 mixture of **1** and **3** and the precipitation of Na_2CO_3. In contrast, when **2** was reacted with CO_2 in toluene, only **1** was isolated and sodium oxalate detected. The reaction of **2** with CO_2 is the first example where the pathway reduction of CO_2 is a function of the solvent [25].

2.4. Carbene functionalities bonded to [Fe(tmtaa)]

The synthesis of the carbene derivative **12** was performed by reacting **1** with the corresponding diazoalkane. The reaction was carried out at −30°C in THF and then at room temperature, and after workup gave a good yield of **12** (Scheme 4).

Complex **12** is diamagnetic and easily characterized by ^{1}H- and ^{13}C-NMR spectroscopies. An X-ray analysis of this compound confirmed the spectroscopic data (Fig. 5). The coordination environment of iron is a distorted tetragonal pyramid, unlike the Fe–porphyrin

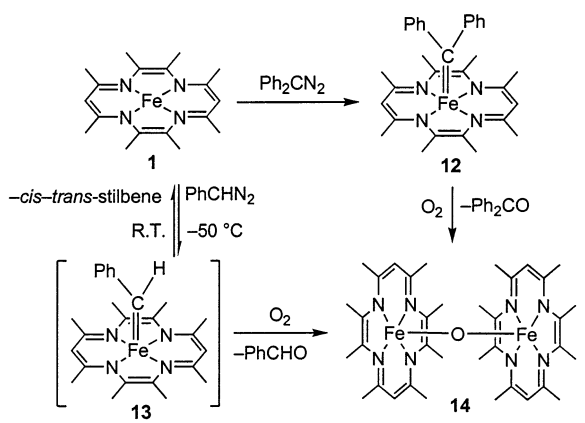

Scheme 4.

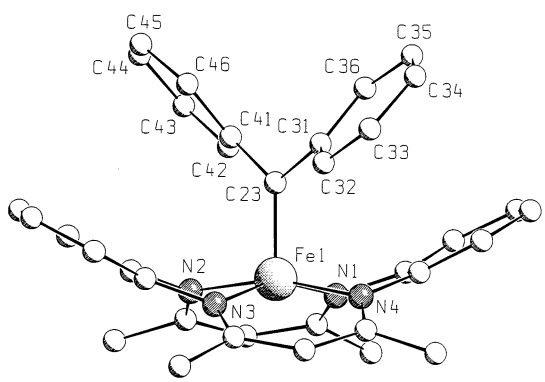

Fig. 5. SCHAKAL view of complex **12**.

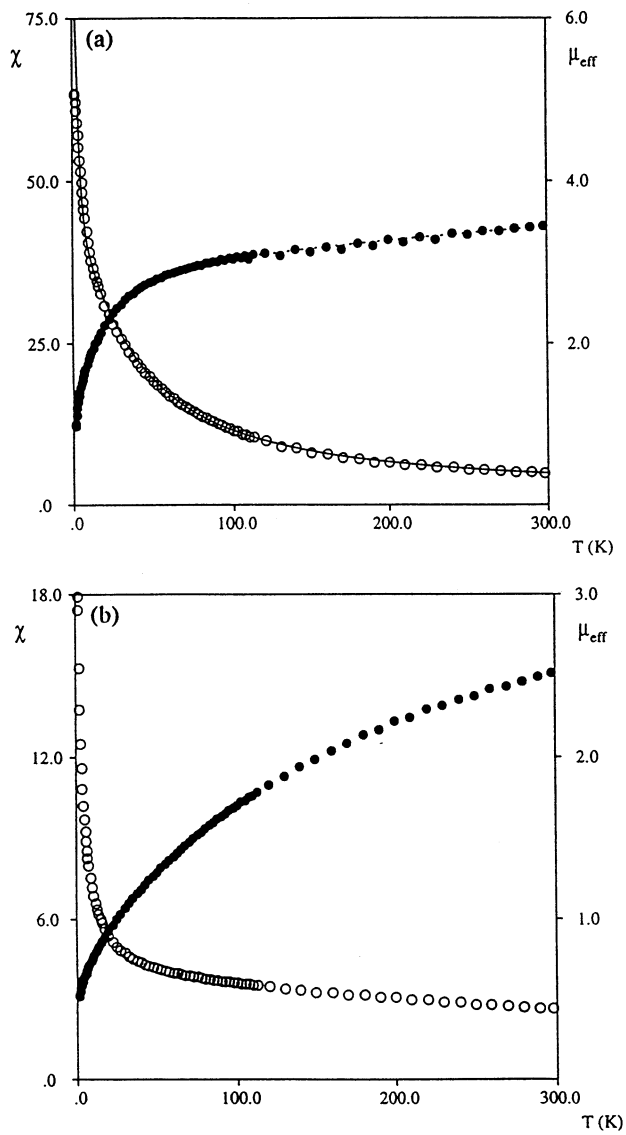

Fig. 6. Magnetic susceptibilities (○) and magnetic moments (●) as a function of the temperature: (a) for complex **1**; (b) for complex **7**.

[9a] and Os–porphyrin [26] examples, where the metal is always hexa-coordinate. The metal is displaced by 0.335(1) Å from the N_4 average plane. The Fe–C(23) vector is perpendicular to the N_4 core, the dihedral angle with the normal to the N_4 plane being 1.0(1)°. The carbene plane C(23),C(31),C(41) is almost parallel to the N(2)···N(4) vector, the torsion angles C(31)–C(23)–Fe–N(4) and C(41)–C(23)–Fe–N(2) being −15.5(3) and −15.2(3)°, respectively. The Fe–C(23) bond distance [1.794(3) Å] is particularly short compared with the only available iron–porphyrin [Fe=CCl_2, 1.83(3) Å] [9a] or the organometallic derivatives of iron, where it ranges from 1.978(3) to 1.85(3) Å [27]. The tmtaa ligand, which shows the usual saddle shape conformation, has structural parameters close to those reported for the other iron complexes (Tables 2 and 3).

The question as to whether the oxidation state of iron in **12** is (II) or (IV) can be reasonably answered, in the absence of Mössbauer measurements, by considering the Fe distance from the N_4 plane. A correlation in tmtaa complexes has been established between the out of plane of the metal and its d^n configuration [2d]. All the M(tmtaa) units presented show the saddle shape conformation with differences depending principally on the metal ion radius and on its oxidation state. The observation is that for electron-rich metals (d^6–d^8), the saddle shape conformation almost disappears and the metals lie in the plane. Metals with d^0 and d^1 configurations, on the other hand, have the most pronounced out-of-plane and saddle shape conformation. The value found in the present case for **12** [0.335(1) Å] is expected for a low-spin d^6 five-coordinate iron(II), i.e. 0.29 Å in [Fe(tmtaa)CO] [11h]. Much longer distances would be found for a d^4 configuration. The extended Hückel calculations (see below) further support the + II oxidation state for iron in **12** and the use of carbene rather than alkylidene terminology for the present complex.

The carbene complex **12** showed a very high thermal stability and even a high resistance to hydrolysis. In order to test the metathesis reaction and polymerization, we reacted **12** with benzophenone, diphenylacetylene and norbornene. In all cases no reaction occurred even under reflux conditions. Oxidation and reduction reactions were then carried out, in order to change the kinetically inert d^6 configuration. When carbene **12** was reacted with dioxygen in THF, the poorly soluble μ-oxo dimer **14** [11o] formed. A GC analysis of the mother liquor shows the presence of benzophenone. In contrast, the reduction of **12** with sodium did not give a well-defined product. The stability and the nature of the final compound derived from the reaction of **1** with diazoalkanes is strongly dependent on the substituents at the carbene carbon. In the case of $PhCHN_2$, the carbene derivative **2** forms only at low temperature. It decomposes at room temperature leading to the starting material, *trans*-stilbene (81%) and *cis*-stilbene (19%) as shown by GC analysis. In the presence of dioxygen at low temperature, benzaldehyde and the μ-oxo dimer **14** are formed (Scheme 4), which proves the formation of the intermediate carbene species at low temperature.

2.5. Magnetic properties

The magnetic susceptibilities of complexes **1**–**11** were collected in the temperature range 1.9–300 K and those of **1**, **2**, **7**–**9**, and **11** are shown in Figs. 6–8.

2.5.1. Iron(II) complexes

The d^6 iron(II) ion can exhibit three spin states, i.e. the $S = 0$ low-spin state, the $S = 1$ intermediate-spin state and the $S = 2$ high-spin state. Although the inter-

mediate spin cannot be observed in an ideal octahedral environment, it has been observed for some tetragonal or severely distorted pyramidal coordinations, see discussion below.

The temperature dependence of the magnetic moments of **1** is illustrated in Fig. 6(a). The magnetic moment is almost constant between 100 and 300 K with a room temperature value of $3.45\mu_B$ at 298 K and shows a sudden decrease below 50 K reaching $0.95\mu_B$ at 2 K. The room temperature value of the effective magnetic moment is consistent with an $S = 1$ intermediate-spin state, while the decrease at low temperature can be attributed to a large zero-field splitting with a non-magnetic level lying lowest. This behavior is quite

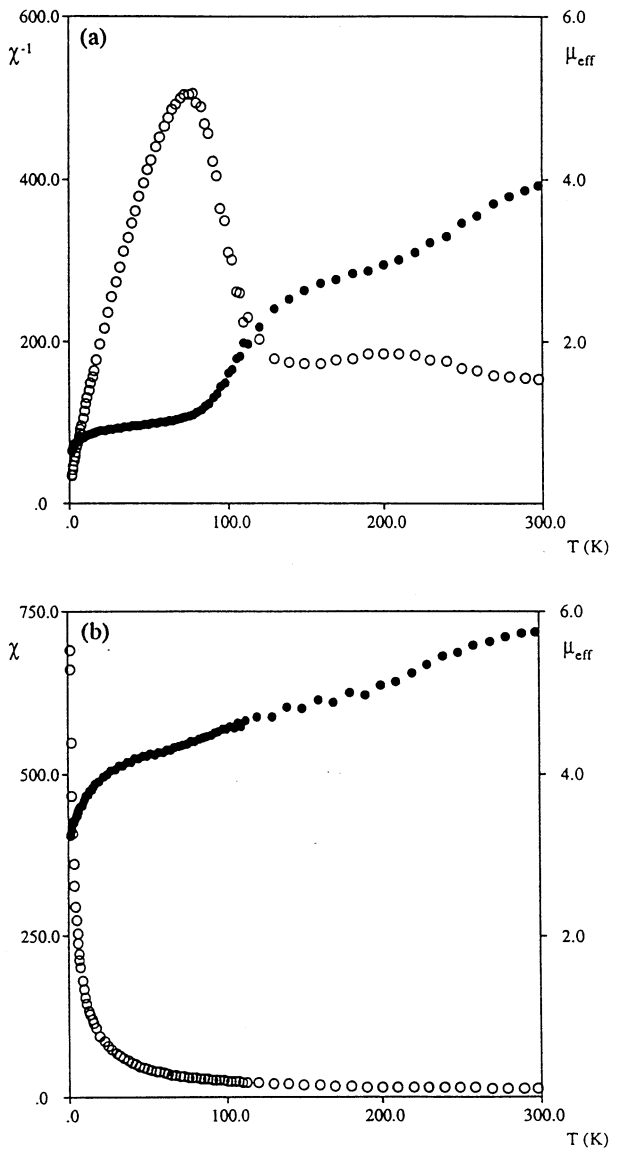

Fig. 7. (a) Inverse magnetic susceptibility (○) and magnetic moment (●) as a function of the temperature for complex **8a**; (b) magnetic susceptibility (○) and magnetic moment (●) as a function of the temperature for complex **9**.

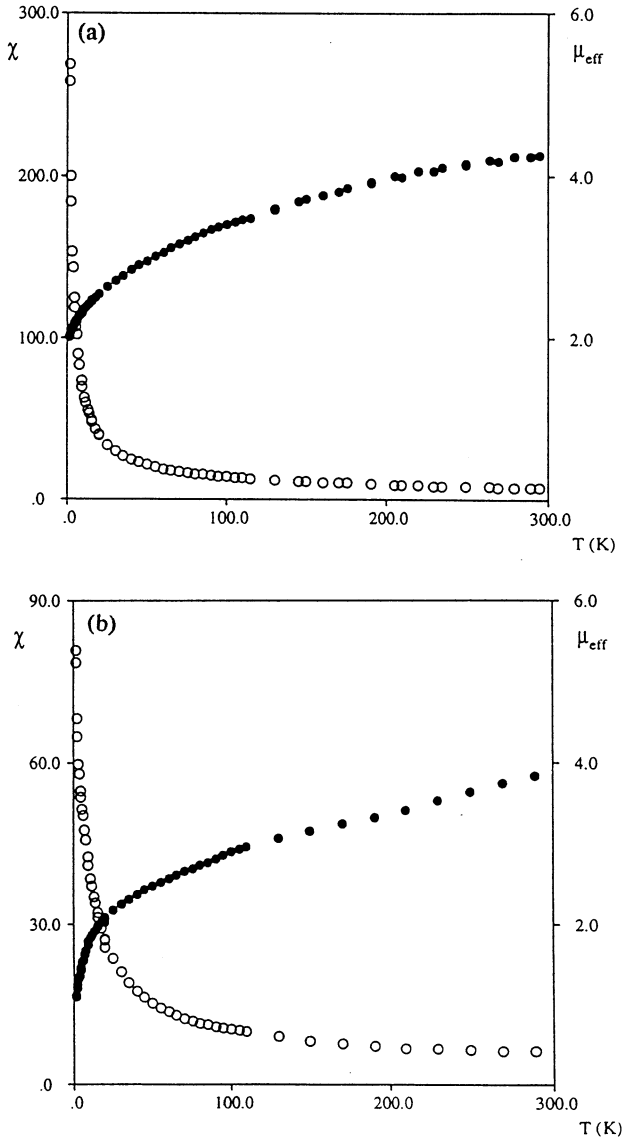

Fig. 8. Magnetic susceptibilities (○) and magnetic moments (●) as a function of the temperature: (a) for complex **2**; (b) for complex **11a**.

similar to that of other tetracoordinated Fe^{II} complexes with a square-planar coordination constituted by a N_4 macrocyclic ligand [28,29]. The room-temperature value of **1** is very close to that reported for Fe(Pc) (Pc = phthalocyanine), $\mu_{eff} = 3.9\mu_B$ [28], and slightly lower than that of Fe(TPP) (TPP = tetraphenylporphyrin), $\mu_{eff} = 4.2\mu_B$ [29]. The magnetic data have been analyzed in terms of an isolated $S = 1$ state with an isotropic g-factor and an axial zero-field splitting described by the following spin hamiltonian [30]: $\boldsymbol{H} = \beta g \boldsymbol{H} \cdot \boldsymbol{S} + D[\boldsymbol{S}_z^2 - S(S+1)/3]$, where $S = 1$ and D is the zero-field splitting constant. The spin degeneracy of the $S = 1$ state is partly lift by spin-orbit coupling into the $M_s = 0$ and $M_s = \pm 1$ components, separated by the zero-field splitting parameter D. The magnetic susceptibility can be derived by using the Van-Vleck equation and is given by [30]

Table 4
Summary of the magnetic properties of [Fe(tmtaa)(L)(L′)] complexes

	L	L′	μ_{eff} (2 K)	μ_{eff} (298 K)	Spin state	Features
1	None	None	0.95	3.45	1	Intermediate-spin
3	CO	THF	0.70	3.10	0↔1	Spin-crossover
4	CO	Py	–	–	0	Diamagnetic
5	CNR [a]	THF	–	–	0	Diamagnetic
6	CN^{t}Bu	THF	–	–	0	Diamagnetic
7	CN^{t}Bu	CN^{t}Bu	0.55	2.55	0↔1	Spin-crossover
8b	CN^-	None	0.60	3.95	0↔1↔2	Spin-crossover
9	CN^-	None	3.20	5.80	1↔2	Spin-crossover
10	Py	Py	0.50	2.40	0↔1	Spin-crossover

[a] R = *o*-$Me_3SiC_6H_4$.

$$\chi_{dim} = \frac{Ng^2\mu_B^2}{kT}\frac{2\exp(-x)+(2/x)\exp(-x)}{1-2\exp(-x)}$$

where $x = D/kT$. A temperature-independent paramagnetism (TIP) contribution has been added to account for the slight decrease between 300 and 100 K. A good fit was found for $g = 2.22$, $D = 42.5$ cm^{-1}, and $N\alpha = 9 \times 10^{-4}$ (see solid line in Fig. 6(a)).

The coordination of one or two axial ligands to **1** changes drastically its magnetic behavior. A summary of the magnetic properties of polycrystalline samples of the characterized [Fe(tmtaa)(L)(L′)] complexes is given in Table 4. We see that most of these compounds are either diamagnetic (**4–6**), although with a little residual paramagnetism due to TIP contribution or to paramagnetic impurities, or show magnetic moments which are compatible with only low or intermediate spin states (**3**, **7**, **10**). Only the cyanide complexes **8** and **9** show magnetic moments compatible with the presence of some high-spin character (see below).

Compounds **3**, **7** and **10** show an uncommon magnetic behavior which is exemplified by the temperature dependence of the magnetic moment for **7** illustrated in Fig. 6(b). The moment of **7** has a value of $2.55\mu_B$ at 298 K, which is slightly lower than that expected for an intermediate spin state, and shows a continuous decrease with temperature reaching a value of 0.55 at 2 K. This behavior is compatible with: (i) an intermediate-spin triplet ground state with a large zero-field splitting; (ii) the presence of a spin crossover involving a low-spin $S = 0$ and an intermediate spin $S = 1$ states. Since the zero-field interaction necessary to cause a decrease of the magnetic moment already at room temperature would be anomalously too high, and it was not possible to fit the magnetic data to either an axial or rhombic spin hamiltonian, we favor the latter explanation, i.e. an $S = 0$–1 spin-crossover.

It is interesting to compare the magnetic behavior of these four-, five-, and six-coordinate iron(II) tetraaza complexes with the related iron(II) porphyrin complexes, whose structural and electronic features have been probed in considerable depth in the past years [31,32].

For the porphyrin complexes the spin state of the iron(II) center is determined by the nature and the number of axial ligands: the coordination of strong-field ligands (Py, CO) leads to low-spin six-coordinate complexes, while the coordination of weaker field ligands (THF, 2-MeIm) leads to high-spin five- or six-coordinate complexes; the absence on any axial ligands leads to a intermediate spin complex. Therefore, the decrease of the axial ligand field give sequentially low-spin, high-spin and intermediate-spin states. These observations have been interpreted in terms of ligand field effects on the d-orbital splitting [32], which for an iron porphyrin is given by three nearly degenerate low-lying d_{xy}, d_{xz}, d_{yz}, the high-lying $d_{x^2-y^2}$ whose lobes point towards the porphyrinato nitrogen atoms, and the d_{z^2} whose energy is affected strongly by the axial ligand field. In particular, the high energy of the $d_{x^2-y^2}$-orbital stabilizes the $(d_{xy})^2(d_{z^2})^2(d_{xz}, d_{yz})^2(d_{x^2-y^2})^0$ intermediate-spin state, while the strong dependence of the d_{z^2}-orbital on the axial ligand field may determine a low-spin or high-spin ground state.

The main difference between the magnetic behavior of the iron(II) porphyrins and our iron(II) tetraaza complexes is the higher occurrence of the intermediate-spin state, while the high-spin state is nearly absent, being observed only in the cyanide compounds **8a** and **9**, and never as ground state. Such an effect can be easily rationalized on the basis of the different sizes of the porphyrin and tetraaza macrocycle coordination cavity [2m]. Indeed, the tetraaza system has only a 14-membered inner ring as compared to the larger 16-membered porphyrin ring and this gives rise to a 1.90–1.93 Å ring size for tetraaza, which is ca. 0.1 Å less than that for the porphyrins. The small ring rises the $d_{x^2-y^2}$-orbital energy well above the other four, thus favoring the low-spin and intermediate-spin states over the high-spin state.

The magnetic behavior of the Na^+-bridged cyanide dimer **8a** is quite peculiar as illustrated by the temperature dependence of the magnetic moment in Fig. 7(a), showing the occurrence of an almost complete double

step spin transition (note the presence of a second maximum in the χ^{-1} versus T plot). Such a magnetic behavior is quite rare, and was first reported in 1969 for the iron(III) compound H[Fe(5-Br–thsa)$_2$] (thsa = 2-bromo-salicylaldheydethiosemicarbazone) [33] and only in 1982 for the iron(II) complex [Fe(2-pic)$_3$Cl$_2$] × EtOH (2-pic = 2-picolylamine) [34]. Since then few rare examples of two-step spin conversions for iron(II) complexes have been described [35–37] and only one involves a dimeric system [36]. Two possible explanation have been proposed for this behavior: (i) the occurrence of the following two transitions LS–LS↔LS–HS↔HS–HS where the two LS (low-spin) or HS (high-spin) states refers to two non-equivalent sites of the lattice [38] or to the two metal centers within the dimer [36a]; and (ii) the occurrence of a two-step transition involving the $S = 0$, $S = 1$ and $S = 2$ spin states of the single metal centers [37]. The former explanation have been proposed in all two-steps spin conversions described to date, except for the recently characterized [Fe(4,4′-dpb)$_2$(NCS)$_2$] complex (4,4′-dpb = 4,4′-diphenyl-2,2′-bipyridine), whose magnetic behavior was interpreted assuming the involvement of the $S = 1$ state [37]. Although the dimeric nature of **8a** would suggest the occurrence of a LS–LS↔LS–HS↔HS–HS transition, the presence of a low-lying intermediate-spin state for most of the characterized [Fe^{II}(tmtaa)(L)(L′)] complexes could allow the more appealing $S = 0 \leftrightarrow S = 1 \leftrightarrow S = 2$ interpretation, and a correct interpretation of the magnetic behavior of **8a** would require further calorimetric and spectroscopic investigations. The magnetic behavior of the monomeric cyanide complex **9** is illustrated in Fig. 7(b) and is indicative of a $S = 1 \leftrightarrow S = 2$ spin transition, therefore supporting the involvement of the $S = 1$ state also in the dimeric complex **8a**. The different nature of the spin states involved in the monomeric and dimeric cyanide complexes is reflected in the remarkable differences of structural parameters and spectroscopic properties. Indeed, at variance with the dimer **8**, which shows a little high-spin character even at room temperature, the monomeric complex **9** has a predominant high-spin character above 100 K and is expected to present longer metal–ligand bond distances and a higher out-of-plane in agreement with the experimental evidence (see Tables 2 and 3). Moreover, the depopulation occurring in the high-spin state of the d_π-orbitals, responsible of the π-back-donation to CN^-, explains the remarkable higher stretching vibration observed for **9** (2089 cm^{-1} vs. 1987 in **8**). The slight ligand field changes induced by the rupture of the dimeric structure probably lead to the destabilization of the low-spin state showing that the spin-state ordering of these iron(II) tmtaa complexes is very sensitive to subtle structural effects.

2.5.2. Iron(I) complexes

Magnetic susceptibilities data for complex **2** are displayed in Fig. 8(a). At room temperature the magnetic moment of **2** (4.15μ_B at 298 K) is almost consistent with a $S = 3/2$ high spin state, whereas the moment decreases at lower temperatures reaching a value of 2.04μ_B at 1.9 K, which is slightly greater than the spin only value for a $S = 1/2$ low spin state. This behavior is quite different from that observed for the iron porphyrin anion [Fe(TPP)]$^-$, which shows an isolated doublet ground state [16a].

In an attempt to rationalize these magnetic data, a few explanations can be given to interpret the anomalous dependence of μ_{eff} on the temperature: (1) a high-spin quartet ground state with weak antiferromagnetic exchange within the solid state structure; (2) a large zero-field splitting of a high-spin quartet ground state into two $M_s = \pm 3/2$ and $M_s = \pm 1/2$ levels; (3) a spin conversion between a doublet and a quartet state; (4) a doublet ground state admixed with a low-lying thermally non-populated quartet. Explanation (1) can already be eliminated on the basis of the X-ray structure, which shows no contact between neighboring spin centers. When we consider explanation (2) we should first note that the temperature dependence of the magnetic moment is not typical of systems in which zero-field effects are observed. Zero-field interactions have usually a magnitude of few cm^{-1} and, as a consequence, μ_{eff} remains constant from room temperature to about 30–60 cm^{-1} showing a decrease only at lower temperatures [30]. Although a large zero-field splitting could be induced by the interaction of the quartet ground state with a low-lying excited state, it was not possible to fit the magnetic data to either an axial or rhombic spin Hamiltonian, so that we can rule out this explanation. The remaining explanation of the magnetic behavior is either the existence of a spin-conversion between an $S = 1/2$ and an $S = 3/2$ state, or a spin-admixed $S = 1/2$–$3/2$ state.

It is noteworthy that the magnetic behavior of complex **2** is similar to that observed for a series of five-coordinated mono-nitrosyl complexes of iron, formally iron(I), with salen (salen = *N*,*N*′-ethylenebissalicylideneiminato) [39,40], or TMC (TMC = 1,4,8,11-tetramethyl-1,4,8,11-tetraazacyclotetradecane) [40] ring-substituted derivatives. These complexes have a magnetic moment at room temperature consistent with three unpaired electrons: one of them (with unsubstituted salen) shows a sharp transition in the μ_{eff} versus temperature curve at ca. 180 K [39], while in the other cases the decrease of the magnetic moment with decreasing temperature was found to be more gradual and qualitatively similar to that observed for **2** [40,41]. The nature of the states involved in the proposed explanations ($S = 1/2 \leftrightarrow S = 3/2$ spin conversion or $S = 1/2$–$3/2$ spin admixed state) can be discussed on the basis of the

qualitative molecular orbital diagram for [Fe(tmtaa)] in Fig. 9, see extended Hückel analysis below. The low-spin state is probably a $(d_{z^2})^2(d_{x^2})^2(d_{y^2})^2(d_{x^2-y^2})^1$ configuration, while the high-spin state could be either a $(d_{z^2})^2(d_{xz})^2(d_{yz})^1(d_{x^2-y^2})^1(d_{xy})^1$, of iron(I) character, or a $(d_{z^2})^2(d_{xz})^2(d_{yz})^1(d_{x^2-y^2})^1(a_2)^1$, or $(d_{z^2})^2(d_{xz})^2$-$(d_{yz})^1(d_{x^2-y^2})^1(b_2)^1$ of iron(II)-π radical anion character. Although the low energy of the a_2 and b_2 orbitals (of π*(tmtaa) character) favors the latter alternative, only further spectroscopic investigations and a theoretical study could clarify this point.

Magnetic susceptibility data for complex **11a** are illustrated in Fig. 8(b). The temperature dependence of the magnetic moment is qualitatively similar to that of **2**, but shows a larger decrease at low temperatures, reaching a value of $1.1\mu_B$ at 1.9 K. This latter value is not consistent with the spin only value for an $S = 1/2$ low-spin state of a magnetically isolated spin center, and would suggest a small antiferromagnetic interaction between the two iron ions within the dimeric unit mediated by the $-C{\equiv}O-Na^+-O{\equiv}C-$ bridge.

2.6. Extended Hückel analysis on iron–tmtaa complexes

Extended Hückel calculations [42] were performed to gain a better understanding of the main electronic and magnetic properties of the iron(I) and iron(II) complexes supported by the dibenzotetramethyltetraazaannulene ligand and to elucidate the nature of the bonding between a carbene unit and the central metal in complexes **12** and **13**. The tmtaa ligand has been simplified by replacing the benzene units by ethylene and the methyl groups by hydrogens, and slightly adjusted to a C_{2v} symmetry. Such a simplified model has already been employed in EH [43] and SCF-X-SW [12d,e] calculations and showed a good correlation with the results obtained with the whole ligand [12d,e].

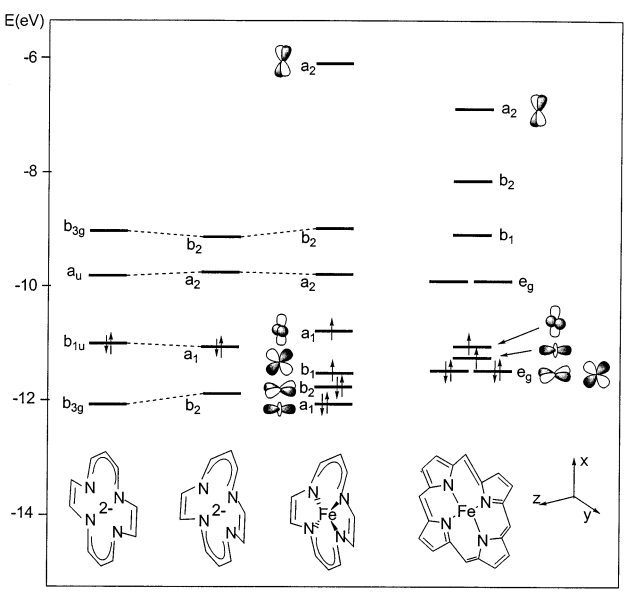

Fig. 9. Orbital interaction diagram for [Fe(tmtaa)(CH_2)].

The molecular orbitals of the [Fe(tmtaa)] fragment are built in a step-by-step approach. We first considered the planar $(tmtaa)^{2-}$ ligand of D_{2h} symmetry, which was then deformed so as to reproduce the geometry of the (tmtaa) skeleton in the final [Fe(tmtaa)(CPh_2)] complex. The molecular orbitals for the planar $(tmtaa)^{2-}$ ligand are reported in the first column of Fig. 9 while in the second one we illustrate the effect of the bending up of the two benzo groups (19.8°) and the bending down of the two allyl groups (26.7°). We finally add Fe in the middle of the (tmtaa) ring and the resulting MO diagram is reported in the third column of Fig. 9. Upon coordination, the d-orbitals mix strongly with the ligand frontier orbitals so that no pure d-orbitals can be assigned. However, five MOs with large metal d character can be identified. These are the four highest occupied orbitals $a_1(d_{z^2})$, $b_2(d_{yz})$, $b_1(d_{xz})$ and $a_1(d_{x^2-y^2})$. The $a_2(d_{xy})$, pointing more closely towards the nitrogen atoms of tmtaa, is pushed very high in energy. The two LUMOs correspond closely to the two LUMOs of the $(tmtaa)^{2-}$ distorted ligand, b_{1g} and a_u.

The molecular orbitals of the [Fe(porphyrin)] fragment have been the subject of several extended Hückel investigations [44], and its molecular fragment are reported on the extreme right of Fig. 9 for purpose of comparison. We see that both [Fe(porphyrin)] and [Fe(tmtaa)] fragments have a very similar d-orbital splitting pattern, the main differences being: (i) the d_{xz} and d_{yz} are no longer degenerate in the tmtaa fragment (due to the lower symmetry), although still very close in energy; (ii) the d_{xy} and the $d_{x^2-y^2}$-orbitals are significantly higher in energy in the tmtaa fragment, essentially as a consequence of the smaller ring size. In particular, this latter difference is responsible of the stabilization of the intermediate-spin state observed for the tmtaa complexes (see above).

We then considered the bonding in the carbene complexes **12** and **13**, using a CH_2 as a model for the carbene unit. The interaction between the [Fe(tmtaa)] fragment and the CH_2 unit is illustrated by the molecular orbital diagram for the [Fe(tmtaa)(CH_2)] complex in Fig. 10. The molecular orbitals of the [Fe(tmtaa)] fragment described above are reported on the left, while on the right we report the frontier orbitals of CH_2, i.e. the σ-donor $a_1(sp^2$ hybrid) and the π-acceptor $b_1(p_y)$. The X-ray structure of the [Fe(tmtaa)CPh_2)] complex **12** shows that the carbene CPh_2 plane forms an angle of about 57° with the *yz* symmetry plane bisecting the benzo groups. However, in order to keep the C_{2v} symmetry of the metal fragment and simplify the analysis of the results we considered a model orientation with the CH_2 plane lying in the *yz* symmetry plane.

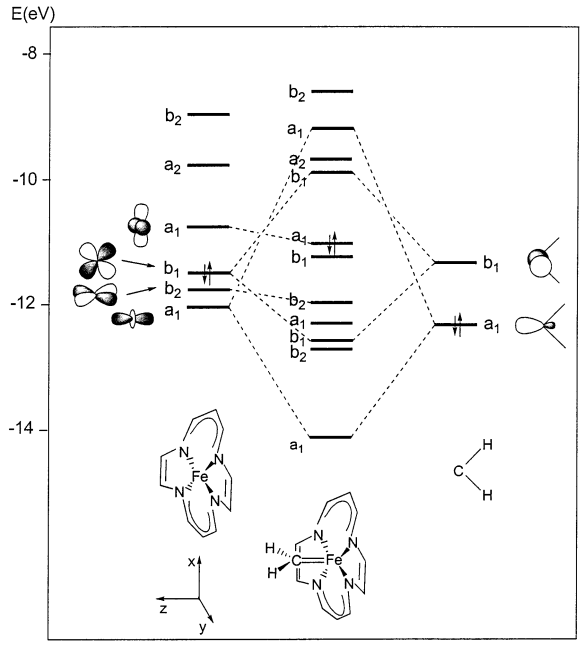

Fig. 10. Molecular orbitals for [Fe(tmtaa)] and [Fe(porphyrin)].

In principle, the π-acceptor orbital of CH_2 could interact with both the doubly occupied $b_1(d_{xz})$, $b_2(d_{yz})$ metal orbitals leading to different orientations of the carbene moiety with the HCH unit lying in the *yz* and *xz* planes, respectively. The former orientation has been calculated ca. 0.3 eV more stable, probably due to the more favorable interaction of the carbene π-acceptor orbital with the higher-lying $1b_1(d_{xz})$ donor orbital and is that reported in Fig. 10. The apparent disagreement with the experimental X-ray structure can be rationalized by noting that the electronically most favorable orientation of the carbene moiety would lead to strong steric repulsion between the two bent benzo groups and the carbene phenyl substituents. The observed orientation is, therefore, a compromise between electronic factors favoring the orientation of the CPh_2 in the *yz* plane and steric repulsion favoring the orientation of the carbene in the *xz* plane.

Fig. 10 shows a strong interaction between the $1a_1(d_z2)$ and the σ-donor $1a_1$ of CH_2, and between the $1b_1(d_{xz})$, and the π-acceptor b_1. These interactions are typical of most of the known metal carbene species [45]. In particular, frontier orbital criteria suggest for this [Fe(tmtaa)(CH_2)] species a Fischer carbene nature rather than a Schrock alkylidene, supporting the used terminology. This is supported by the low energy of the metal d_π-orbitals, lower than that of the π-acceptor b_2-orbitals, and the presence of a low-lying LUMO (see Fig. 10), which gives a significant electrophilic character to the carbene moiety, both effects being characteristic of Fischer carbene systems. However, the carbene unit shows a small, negative charge on the carbon atom (-0.05) and a significant population of the π-acceptor b_2, which would be more typical of Schrock alkylidenes. Therefore, compounds **12**–**13** can be actually described as intermediate between a Fischer carbene and a Schrock alkylidene without a definite electrophilic or nucleophilic character of the carbene carbon. The negligible electron donation of the [Fe(tmtaa)] fragment to the CH_2 moiety upon carbene formation (0.1 e) supports the attribution a formal oxidation state of $+2$ and a d^6 configuration for iron, the same as [Fe(tmtaa)], based on geometrical evidences (see above).

3. Conclusions

The [Fe(tmtaa)] fragments showed a great versatility in binding π-acid ligands from CO to RNC, CN and carbenes, displaying a wide spectrum of magnetic behaviors, which depend on the coordination number of the metal and the axial ligand. A remarkable difference has been observed between the monomeric and the sodium-bridged dimeric cyano complexes in terms of magnetic behavior. This result emphasizes the primary role of alkali cations in determining not only the molecular complexity, but also the physical properties. A unique structural model of diamagnetic iron(II)–carbene complexes has been reported. A quite rare d^7-iron(I)-macrocycle occurring in an ion-pair form has been synthesized and structurally characterized and its reactivity with CO and CO_2 explored. In the former case, a quite unique carbonyl dimer bridged by sodium cation was identified, while in case of CO_2, for the first time, the solvent-dependence of the reduction of CO_2 has been singled out.

4. Experimental

4.1. General procedures

All reactions were carried out under an atmosphere of purified nitrogen. Solvents were dried and distilled before use by standard methods. Infrared spectra were recorded with a Perkin–Elmer FT 1600 spectrophotometer, UV–vis spectra were recorded with a Hewlett–Packard 8452A diode array spectrophotometer, NMR spectra were recorded on AC-200E and DPX-400 Bruker instrument. The synthesis of tmtaaH_2 ligand has been carried out according to the literature [46].

Magnetic susceptibility measurements were made on an MPMS5 SQUID susceptometer (Quantum Design), operating at a magnetic field strength of 1 kOe. Corrections were applied for diamagnetism calculated from Pascal constants [47]. Effective magnetic moments were calculated as $\mu_{eff} = 2.828(\chi_{Fe}T)^{1/2}$ were χ_{Fe} is the magnetic susceptibility per iron. Fitting of the magnetic data to the theoretical expression were performed by minimizing the agreement factor, defined as

$$\sum \frac{[\chi_i^{obsd} T_i - \chi_i^{calcd} T_i]^2}{(\chi_i^{obsd} T_i)^2}$$

by a Levenberg–Marquardt routine.

4.2. Synthesis of **1**

A solution of butyllithium (63 ml, 1.63 M, 102 mmol) in *n*-hexane was added to a THF solution (550 ml) of tmtaaH_2 (17.6 g, 51.1 mmol) at room temperature (r.t.). The reaction was exothermic and became red. After stirring for 3 h, [$FeCl_2 \times THF_{1.5}$] (12.0 g, 51.1 mmol) was added and then stirred overnight at −20°C. The resulting purple microcrystalline solid was filtered and dried in vacuo (16.9 g, 71%). No extraction was needed to remove the salt. (Found: C, 66.45; H, 6.52; N, 12.3%. **1**·THF, $C_{26}H_{30}FeN_4O$ requires C, 66.39; H, 6.43; N, 11.91%.) IR (Nujol, ν_{max}/cm^{-1}): 1578 (w), 1508 (s), 1463 (s), 1398 (s), 1278 (m), 1198 (s), 1053 (w), 1034 (m), 920 (w), 787 (m), 772 (m), 749 (s), 535 (w). ^{1}H-NMR (C_5D_5N, 200 MHz, 298 K, ppm): δ 6.45 (bs, 4H, Ar); 6.18 (bs, 4H, Ar); 3.48 (bs, 2H, CH); 1.59 (bs, 12H, CH_3). $\mu_{eff} = 3.45\mu_B$ at 298 K.

4.3. Synthesis of **2**

Sodium sand (0.478 g, 20.8 mmol) was added to a THF suspension (240 ml) of **1**·THF (8.1 g, 17.2 mmol) and the mixture was stirred for 10 h. The green solution was warmed (ca. 40°C) to complete solubilization and then filtered. The solvent was reduced in vacuo to 20 ml and *n*-hexane (20 ml) was then added. The black crystalline solid was filtered and dried in vacuo (8.6 g, 78%). (Found: C, 64.26; H, 7.30; N, 8.68%. **2**, $C_{34}H_{46}FeN_4NaO_3$ requires C, 64.05; H, 7.27; N, 8.79%.) IR (Nujol, ν_{max}/cm^{-1}): 1385 (s), 1340 (m), 1269 (m), 1182 (w), 1049 (m), 823 (w), 737 (m), 588 (w). $\mu_{eff} = 4.15\mu_B$ at 298 K.

4.4. Synthesis of **3**

A THF solution (150 ml) of **1** × THF (2.49 g, 5.29 mmol) was saturated with CO at r.t. A sudden reaction was observed and the solution became red. The solvent volume was reduced to 10 ml and *n*-hexane (25 ml) added. The crystalline material was filtered and dried in vacuo (2.0 g, 75%). (Found: C, 64.99; H, 6.02; N, 11.34%. **3**, $C_{27}H_{30}FeN_4O_2$ requires C, 65.07; H, 6.07; N, 11.27%.) IR (Nujol, ν_{max}/cm^{-1}): 1913 (s, CO), 1577 (w), 1531 (m), 1378 (s), 1282 (w), 1198 (m), 1034 (m), 785 (w), 740 (m). ^{1}H-NMR (C_5D_5N, 200 MHz, 298 K, ppm): δ 6.59–6.56 (m, 4H, Ar); 6.47–6.43 (m, 4H, Ar); 6.01–5.99 (m, 0.4H); 4.14 (s, 2H, CH); 3.69 (m, 4H, THF); 1.79 (s, 12H, CH_3); 1.58 (m, 4H, THF); 1.30 (s, 1.6H). $\mu_{eff} = 3.10\mu_B$ at 298 K.

4.5. Synthesis of **4**

Pyridine (1.0 ml, 12.4 mmol) was added to a stirred THF solution (100 ml) of **1**·THF (1.53 g, 3.25 mmol). After 15 min, the blue solution was saturated with CO with a concomitant color change to red. Stirring was maintained overnight and the solution then concentrated (20 ml). *n*-Hexane was then added (30 ml) and the crude product filtered and dried in vacuo (1.31 g, 80%). It was recrystallized in acetonitrile. (Found: C, 66.48; H, 5.23; N, 13.29%. **4**, $C_{28}H_{27}FeN_5O$ requires: C, 66.54; H, 5.38; N, 13.86%.) IR (Nujol, ν_{max}/cm^{-1}): 1927 (s, CO), 1599 (w), 1571 (w), 1518 (s), 1402 (s), 1284 (m), 1199 (s), 1034 (s), 762 (s), 733 (m), 695 (w), 525 (w). ^{1}H-NMR (C_5D_5N, 200 MHz, 298 K, ppm): δ 6.59–6.56 (m, 4H, Ar); 6.47–6.42 (m, 4H, Ar); 6.08–6.04 (m, 0.5H); 4.93 (s, 0.13H); 4.14 (s, 2H, CH); 1.79 (s, 12H, CH_3); 1.41 (s, 2H). ^{13}C-NMR (C_6D_6, 100.6 MHz, 298 K, ppm): δ 235.2 (CO), 159.8, 153.7, 124.3, 123.4, 113.4, 26.2.

4.6. Synthesis of **5**

(*o*-Me_3Si)PhNC (0.95 g, 4.92 mmol) was added via syringe to a cooled (−25°C) THF solution (130 ml) of **1**·THF (2.32 g, 4.92 mmol). A rapid color change was observed and the solution was allowed to warm to r.t. After stirring overnight, the solvent was reduced to 5 ml and *n*-hexane (30 ml) slowly added. The microcrystalline product was filtered and dried in vacuo (2.38 g, 83%). (Found: C, 65.38; H, 5.94; N, 11.88%. **5**, $C_{32}H_{35}FeN_5Osi$ requires: C, 65.19; H, 5.98; N, 11.88%.) IR (Nujol, ν_{max}/cm^{-1}): 2037 (s, NC), 1588 (w), 1519 (m), 1487 (m), 1291 (m), 1251 (m), 1196 (s), 1105 (w), 1032 (m), 915 (s), 844 (s), 746 (s), 595 (w). ^{1}H-NMR (C_6D_6, 200 MHz, 298 K, ppm): δ 7.01–6.51 (m, 12H, Ar); 4.85 (s, 2H, CH); 2.21 (s, 12H, CH_3); 0.09 (s, 9H, Me_3). ^{13}C-NMR (C_5D_5N, 100.6 MHz, 298 K, ppm): δ 205.3 (CN), 158.3, 151.6, 147.8, 130.0, 126.3, 126.0, 121.9, 121.4, 121.2, 120.9, 108.2, 24.6.

4.7. Synthesis of **6**, Method A

A THF solution (40 ml) of ^{t}BuNC (0.38 g, 4.54 mmol) was added dropwise to a cooled (−30°C) THF solution (150 ml) of **1**·THF (2.14 g, 4.54 mmol). The solution was allowed to reach r.t. and then stirred overnight. A microcrystalline product of low solubility precipitated. The solvent was reduced to 25 ml and the solid filtered, washed with *n*-hexane (30 ml) and dried in vacuo (1.66 g, 66%). (Found: C, 67.52; H, 7.22; N, 13.25. **6**, $C_{31}H_{39}FeN_5O$ requires: C, 67.27; H, 7.10; N, 12.65%.) IR (Nujol, ν_{max}/cm^{-1}): 1989 (s, NC), 1570 (w), 1538 (s), 1515 (m), 1430 (s), 1283 (m), 1194 (s), 1033 (s). ^{1}H-NMR (C_5D_5N, 200 MHz, 298 K, ppm): δ 6.52–6.45 (m, 8H, Ar); 6.18 (bs, 0.5H); 4.95 (s, 0.6H);

3.90 (s, 2H, CH); 3.63 (m, 4H, THF); 1.69 (s, 12H, CH_3); 1.58 (m, 4H, THF); 1.39 (s, 9H, ^{t}Bu). ^{13}C-NMR (C_5D_5N, 100.6 MHz, 298 K, ppm): δ 194.6 (CN), 155.2, 153.3, 120.7, 120.1, 119.5, 110.6, 32.0, 23.6.

4.8. Synthesis of **6**, Method B (reaction of **3** with ^{t}BuNC)

A THF solution (30 ml) of ^{t}BuNC (0.13 g, 1.6 mmol)was added dropwise to a red THF solution (100 ml) of **3** (0.73 g, 1.5 mmol). The solution slowly became purple and was stirred for 12 h. The solvent was reduced to 30 ml and *n*-hexane (25 ml) added. The resulting crystalline product was filtered and dried in vacuo (0.51 g, 63%). The analysis showed the product to be **6**. IR and NMR spectra were identical to those above.

4.9. Synthesis of **7**

A THF solution (50 ml) of ^{t}BuNC (0.90 g, 11.0 mmol) was added dropwise to a THF solution (150 ml) of **1**·THF (2.37 g, 5.04 mmol). At approximately half the addition the crystalline **6** precipitated, then redissolved and was stirred for 6 h. Solvent was reduced to 20 ml and *n*-hexane (30 ml) added. The crystalline material was filtered and dried in vacuo (2.23 g, 81%). (Found: C, 67.89; H, 7.36; N, 14.49%. **7**, $C_{32}H_{40}FeN_6$ requires C, 68.08; H, 7.14; N, 14.89%). IR (Nujol, ν_{max}/cm^{-1}): 2156 (m), 2089 (s, CN), 1564 (w), 1535 (m), 1407 (s), 1283 (w), 1190 (s), 1032 (m), 746 (m). ^{1}H-NMR (C_6D_6, 400 MHz, 298 K, ppm): δ 6.47–6.44 (m, 4H, Ar); 6.39–6.37 (m, 4H, Ar); 4.19 (s, 2H, CH); 1.71 (s, 12H, CH_3); 1.32 (s, 18H, ^{t}Bu). ^{13}C-NMR (C_6D_6, 100.6 MHz, 298 K, ppm): δ 178.9 (CN), 155.4, 153.5, 120.3, 119.9, 110.8, 56.5, 31.3, 23.3. $\mu_{eff} = 2.55\mu_B$ at 298 K.

4.10. Synthesis of **8**, Method A

Degassed NaCN (0.14 g, 2.80 mmol) was added to a THF solution (120 ml) of **1**·THF (1.68 g, 2.72 mmol). The solution was allowed to reach reflux conditions during which time the NaCN suspension dissolved (ca. 15 h). The solution was then filtered and solvent removed in vacuo to 10 ml. *n*-Hexane (12 ml) was added and the microcrystalline solid filtered and dried in vacuo (1.75 g, 97%). (Found: C, 63.02; H, 7.24; N, 10.10%. **8a**, $C_{35}H_{46}FeN_5NaO_3$ requires C, 63.35; H, 6.99; N, 10.55%.) IR (Nujol, ν_{max}/cm^{-1}): 1987 (m, CN), 1531 (m), 1511 (m), 1401 (s), 1278 (m), 1189 (s), 1052 (m), 1030 (m), 918 (w), 744 (s). ^{1}H-NMR (C_5D_5N, 200 MHz, 298 K, ppm): δ 6.53–6.49 (m, 4H, Ar); 6.30–6.25 (m, 4H, Ar); 3.91 (s, 2H, CH); 3.67 (m, 8H, THF); 1.71 (s, 12H, CH_3); 1.6 (m, 8H, THF). $\mu_{eff} = 3.95\mu_B$ at 298 K. Crystals suitable for X-ray analysis were grown in DME, as **8b**·DME.

4.11. Synthesis of **8**, Method B (reaction of **6** with sodium)

Sodium (0.062 g, 2.66 mmol) was added to a THF suspension (150 ml) of **6** (1.28 g, 2.32 mmol). Stirring overnight resulted in a brown–red solution, which was then filtered, concentrated to 10 ml, and *n*-hexane (30 ml) added. The microcrystalline solid was filtered and dried in vacuo (0.58 g, 37%). The analysis showed the product to be **8a** (EA, IR, NMR, see above).

4.12. Synthesis of **9**

$Bu_4N^+CN^-$ (2.40 g, 8.90 mmol) was added to a THF solution (250 ml) of **1**·THF (3.56 g, 7.60 mmol). The solution was stirred overnight, then the solvent was evaporated. A red crystalline product was obtained, which was filtered and dried in vacuo (4.51 g, 89%). (Found: C, 69.56; H, 8.98; N, 10.27%. **9**·2THF, $C_{47}H_{74}FeN_6O_2$ requires C, 69.54; H, 9.12; N, 10.36%.) IR (Nujol, ν_{max}/cm^{-1}): 2089 (m), 2011 (w), 1535 (m), 1506 (m), 1400 (s), 1269 (m), 1185 (s), 1026 (m), 922 (w), 734 (m). $\mu_{eff} = 5.80\mu_B$ at 298 K.

4.13. Reaction of **2** with CO_2: (A) reaction in THF

A cooled (-30°C) THF solution (100 ml) of **2** (0.93 g, 1.46 mmol) was saturated with CO_2. A sudden color change to red was observed. The solution was allowed to warm to r.t. and stirred for 3 h. The viscous Na_2CO_3 precipitate was filtered and the solution concentrated to 5 ml. *n*-Hexane (20 ml) was added after which the microcrystalline product was filtered and dried in vacuo (0.525 g). The ^{1}H-NMR showed a 1/1 mixture of **1**·THF (a) and **3** (b) and the IR spectrum was identical to the latter. IR (Nujol, ν_{max}/cm^{-1}): 1913 (s), 1578 (w), 1531 (s), 1281 (m), 1198 (s), 1034 (s), 786 (w), 749 (s). ^{1}H-NMR (C_5D_5N, 200 MHz, 298 K, ppm): δ 6.62–6.57 (m, 4H, Ar, b); 6.50–6.43 (m, 8H, Ar, a + b); 6.25–6.20 (m, 4H, Ar, a); 4.15 (s, 2H, CH, b); 3.76 (s, 2H, CH, a); 3.64 (m, 4H, THF); 1.80 (s, 12H, CH_3, b); 1.66 (s, 12H, CH_3, a); 1.59 (m, 4H, THF). [a = Fe(tmtaa) and b = Fe(tmtaa)CO].

4.14. Reaction of **2** with CO_2: (B) reaction in toluene

A cooled (-30°C) toluene solution (120 ml) of **2** (1.39 g, 2.18 mmol) was saturated with CO_2. A sudden color change to violet–red was observed. The solution was allowed to warm to r.t. and stirred overnight. Solvent was reduced to 30 ml and the microcrystalline product collected and dried in vacuo (0.53 g, 61%). The IR and ^{1}H-NMR spectra were identical to **1**. (Found: C, 66.59; H, 5.31; N, 14.01%. $C_{22}H_{22}N_4Fe$ requires C, 66.34; H, 5.57; N, 14.07%.) IR (Nujol, ν_{max}/cm^{-1}): 1577 (w), 1508 (m), 1278 (m), 1198 (m), 1034 (m), 787

(w), 749 (s). ^{1}H-NMR (C_5D_5N, 200 MHz, 298 K, ppm): δ 6.46 (bs, 4H, Ar); 6.21 (bs, 4H, Ar); 3.50 (bs, 2H, CH); 1.61 (s, 12H, CH_3). In order to detect the presence of sodium oxalate, the mother liquor was extracted with water (2×40 ml), separated and filtered. Activated carbon was added to the brown solution and stirred overnight. Filtration gave a pale brown solution, which was titrated with $KMnO_4$ (0.02 M).

4.15. Synthesis of **11**, Method A

A cooled (-30°C) THF solution (350 ml) of **2** (6.19 g, 9.71 mmol) was saturated with CO. The solution rapidly turned brown. After stirring overnight under CO, the solution was concentrated (40 ml) and *n*-hexane (30 ml) added. The crystalline product was then filtered and dried in vacuo (4.44 g, 77%). (Found: C, 62.62; H, 6.84; N, 9.07%. **11a**, $C_{62}H_{76}Fe_2N_8Na_2O_6$ requires C, 62.74; H, 6.45; N, 9.44%.) IR (Nujol, ν_{max}/cm^{-1}): 1918 (w), 1736 (s, CO), 1536 (m), 1410 (s), 1277 (w), 1188 (s), 1048 (m), 1027 (m), 906 (w), 743 (m). $\mu_{eff} = 3.90\mu_B$ at 298 K. Crystals for X-ray analysis were obtained from DME/toluene as **11b**·$6C_6H_6$.

4.16. Synthesis of **11**, Method B (reaction of (**3**) with sodium)

Sodium sand (0.11 g, 4.7 mmol) was added to a THF solution (150 ml) of **3** (1.9 g, 3.8 mmol). After 30 min, the solution became brown. After stirring overnight, the excess sodium was removed by filtration, and the filtrate concentrated to 10 ml. *n*-Hexane (30 ml) was then added dropwise, and the black microcrystalline solid filtered and dried in vacuo (1.49 g, 66%). The product analyzed as **11a** (EA, IR, NMR, see above).

4.17. Synthesis of **12**

A THF solution (40 ml) of diphenyldiazomethane (0.78 g, 4.0 mmol) was added dropwise to a cooled (-30°C) THF solution (140 ml) of **1**·THF (1.79 g, 3.8 mmol). When warmed to r.t., the solution became red. Nitrogen gas was slowly given off. After stirring for 2 days, the green solution was concentrated in vacuo (20 ml) and then *n*-hexane (15 ml) was added. A green crystalline material was obtained (1.7 g, 75%). (Found: C, 74.53; H, 5.77; N, 9.91%. **12**, $C_{35}H_{32}FeN_4$ requires C, 74.47; H, 5.71; N, 9.92%.) IR (Nujol, ν_{max}/cm^{-1}): 1576 (w), 1515 (m), 1386 (s), 1307 (w), 1279 (w), 1194 (m), 1028 (m), 745 (s), 696 (m), 667 (w). ^{1}H-NMR (C_6D_6, 200 MHz, 298 K, ppm): δ 6.88–6.76 (m, 8H, Ar); 6.35–6.33 (m, 10H, Ph); 5.13 (s, 2H, CH); 2.12 (s, 12H, CH_3). ^{13}C-NMR (C_6D_6, 100.6 MHz, 298 K, ppm): δ 313.2 (C carbene), 166.6, 157.9, 149.3, 127.1, 124.8, 120.9, 120.5, 119.7, 107.3, 67.8, 25.8, 23.2. Crystals suitable for X-ray analysis were grown in toluene and contain one molecule of toluene.

4.18. Reaction of **12** with O_2

Dry oxygen was allowed to diffuse slowly from an adjoining round-bottom flask to a THF solution (100 ml) of **12** (0.99 g, 1.8 mmol). After 2 days a brown solid precipitated (0.61 g, 86%), which analyzed as [Fe(tmtaa)]$_2$O [11o]. A GC analysis of the mother liquor showed the presence of benzophenone.

4.19. Synthesis of **13**

Freshly prepared phenyldiazomethane (0.63 g, 5.4 mmol) was added to a cooled (-30°C) THF solution (150 ml) of **1**·THF (2.14 g, 4.55 mmol). The solution rapidly turned brown with the concomitant evolution of nitrogen gas. The solution was allowed to warm to r.t. and then stirred overnight. The solvent was removed in vacuo (10 ml) and *n*-hexane (20 ml) was added. The purple product (1.03 g, 49%) analyzed as [Fe(tmtaa)] (IR, NMR). A GC analysis of the mother liquor showed the presence of *cis*- and *trans*-stilbene (19 and 81%, respectively).

4.20. Reaction of **13** with O_2

Freshly prepared phenyldiazomethane (0.15 g, 1.26 mmol) was added to a cooled (-50°C) THF solution (80 ml) of **1**·THF (0.49 g, 1.03 mmol). The solution rapidly became brown with the concomitant evolution of nitrogen gas. The solution was stirred for 10 min at this temperature and was then saturated with oxygen. After 10 min the solution was allowed to warm to r.t. and stirred overnight. A brown solid precipitated, which analyzed as [Fe(tmtaa)]$_2$O [11o]. A GC analysis of the mother liquor showed the presence of benzaldehyde and no traces of stilbene.

4.21. X-ray experimental

Single crystals suitable for X-ray diffraction were grown from common organic solvents (Table 1). Data for **2** were collected on a MAR345 image plate, for **8**, **9**, **12** on a Rigaku AFC6S diffractometer, while those for **11** were collected on a Kuma CCD using Mo–K_α radiation. The solutions and refinements were carried out using the programs SHELX-76 [48] and SHELXL-93 [49].

5. Supplementary material

Crystallographic data (excluding structure factors) for the structures reported in this paper have been deposited with the Cambridge Crystallographic Data Centre as supplementary publication nos. CCDC-125018 for **2**, CCDC-125019 for **8**, CCDC-125020 for **9,**

CCDC-125021 for **11,** CCDC-125022 for **12**. Copies of the data can be obtained free of charge from The Director, CCDC, 12 Union Road, Cambridge CB2 1EZ, UK (fax: +44-1223-336-033; e-mail: deposit@ccdc.cam.ac.uk or http://www.ccdc.cam.ac.uk).

Acknowledgements

We thank the 'Fonds National Suisse de la Recherche Scientifique' (Bern, Switzerland, grant no. 20-53336.98), and Fondation Herbette (University of Lausanne, N.R.) for financial support.

References

[1] For leading references on organometallic chemistry based on macrocyclic ligands, see Refs. 2–7.

[2] For tmtaa [dibenzotetramethyltetraaza[14]annulene], see: (a) V.L. Goedken, J.A. Ladd, J. Chem. Soc. Chem. Commun. (1981) 910 and (1982) 142. (b) C. Floriani, S. Ciurli, A. Chiesi-Villa, C. Guastini, Angew. Chem. Int. Ed. Engl. 26 (1987) 70. (c) E. Solari, S. De Angelis, C. Floriani, A. Chiesi-Villa, C. Rizzoli, Inorg. Chem. 31 (1992) 96. (d) S. De Angelis, E. Solari, E. Gallo, C. Floriani, A. Chiesi-Villa, C. Rizzoli, Inorg. Chem. 31 (1992) 2520. (e) L. Giannini, E. Solari, C. Floriani, A. Chiesi-Villa, C. Rizzoli, Angew. Chem. Int. Ed. Engl. 33 (1994) 2204. (f) L. Giannini, E. Solari, S. De Angelis, T.R. Ward, C. Floriani, A. Chiesi-Villa, C. Rizzoli, J. Am. Chem. Soc. 117 (1995) 5801. (g) D.G. Black, D.C. Swenson, R.F. Jordan, Organometallics 14 (1995) 3539. (h) A.J. Blake, P. Mountford, G.I. Nikonov, D. Swallow, Chem. Commun. (Cambridge) (1996) 1835. (i) H. Schumann, Inorg. Chem. 35 (1996) 1808. (j) G.I. Nikonov, A.J. Blake, P. Mountford, Inorg. Chem. 36 (1997) 1107. (k) D.G. Black, R.F. Jordan, R.D. Rogers, Inorg. Chem. 36 (1997) 103. (l) A. Martin, R. Uhrhammer, T.G. Gardner, R.F. Jordan, Organometallics 17 (1998) 382. (m) P. Mountford, Chem. Soc. Rev. 27 (1998) 105.

[3] For porphyrins, see: (a) H. Brand, J. Arnold, Angew. Chem. Int. Ed. Engl. 33 (1994) 95. (b) H. Brand, J. Arnold, Organometallics 12 (1993) 3655. (c) H.-J. Kim, D. Whang, K. Kim, Y. Do, Inorg. Chem. 32 (1993) 360. (d) J. Arnold, S.E. Johnson, C.B. Knobler, M.F. Hawthorne, J. Am. Chem. Soc. 114 (1992) 3996. (e) H. Brand, J. Arnold, J. Am. Chem. Soc. 114 (1992) 2266. (f) H. Brand, J. Arnold, Coord. Chem. Rev. 140 (1995) 137. (g) T. Aida, S. Inoue, Acc. Chem. Res. 29 (1996) 39. (h) J.P. Collman, C.E. Barnes, P.N. Swepston, J.A. Ibers, J. Am. Chem. Soc. 106 (1984) 3500. (i) J.P. Collman, P.J. Brothers, L. McElwee-White, E. Rose, L.J. Wright, J. Am. Chem. Soc. 107 (1985) 4570. (j) J.P. Collman, P.J. Brothers, L. McElwee-White, E. Rose, J. Am. Chem. Soc. 107 (1985) 6110.

[4] For calix[4]arenes, see: (a) L. Giannini, E. Solari, A. Zanotti-Gerosa, C. Floriani, A. Chiesi-Villa, C. Rizzoli, Angew. Chem. Int. Ed. Engl. 35 (1996) 85. Angew. Chem. Int. Ed. Engl. 35 (1996) 2825; Angew. Chem., Int. Ed. Engl. 36 (1997) 753. (b) B. Castellano, A. Zanotti-Gerosa, E. Solari, C. Floriani, A. Chiesi-Villa, C. Rizzoli, Organometallics 15 (1996) 4894. (c) L. Giannini, A. Caselli, E. Solari, C. Floriani, A. Chiesi-Villa, C. Rizzoli, N. Re, A. Sgamellotti, J. Am. Chem. Soc. 119 (1997) 9198 and 9709. (d) A. Caselli, L. Giannini, E. Solari, C. Floriani, N. Re, A. Chiesi-Villa, C. Rizzoli, Organometallics 16 (1997) 5457. (e) A. Zanotti-Gerosa, E. Solari, L. Giannini, C. Floriani, A. Chiesi-Villa, C. Rizzoli, J. Am. Chem. Soc. 120 (1998) 437. (f) L. Giannini, E. Solari, C. Floriani, A. Chiesi-Villa, C. Rizzoli, J. Am. Chem. Soc. 120 (1998) 823.

[5] For metal–porphyrinogen: (a) C. Floriani, Pure Appl. Chem. 68 (1996) 1. (b) D. Jacoby, S. Isoz, C. Floriani, A. Chiesi-Villa, C. Rizzoli, J. Am. Chem. Soc. 117 (1995) 2805. (c) S. Isoz, C. Floriani, K. Schenk, A. Chiesi-Villa, C. Rizzoli, Organometallics 15 (1996) 337. (d) C.M. Kretz, E. Gallo, E. Solari, C. Floriani, A. Chiesi-Villa, C. Rizzoli, J. Am. Chem. Soc. 116 (1994) 10775. (e) S. De Angelis, E. Solari, C. Floriani, A. Chiesi-Villa, C. Rizzoli, Angew. Chem. Int. Ed. Engl. 34 (1995) 1092. (f) S. De Angelis, E. Solari, C. Floriani, A. Chiesi-Villa, C. Rizzoli, Organometallics 14 (1995) 4505. (g) D. Jacoby, S. Isoz, C. Floriani, K. Schenk, A. Chiesi-Villa, C. Rizzoli, Organometallics 14 (1995) 4816. (h) G. Solari, E. Solari, C. Floriani, A. Chiesi-Villa, C. Rizzoli, Organometallics 16 (1997) 508.

[6] For metal–Schiff base complexes: (a) S. Gambarotta, M. Mazzanti, C. Floriani, A. Chiesi-Villa, C. Guastini, J. Chem. Soc. Chem. Commun. (1985) 829. (b) C. Floriani, E. Solari, F. Corazza, A. Chiesi-Villa, C. Guastini, Angew. Chem. Int. Ed. Engl. 28 (1989) 64. (c) F. Corazza, E. Solari, C. Floriani, A. Chiesi-Villa, C. Guastini, J. Chem. Soc. Dalton Trans. (1990) 1335. (d) J.-M. Rosset, C. Floriani, M. Mazzanti, A. Chiesi-Villa, C. Guastini, Inorg. Chem. 29 (1990) 3991. (e) E. Solari, C. Floriani, A. Chiesi-Villa, C. Rizzoli, J. Chem. Soc. Dalton Trans. (1992) 367.

[7] For metal tropocoronand complexes, see: (a) M.J. Scott, S.J. Lippard, J. Am. Chem. Soc. 119 (1997) 3411. (b) M.J. Scott, S.J. Lippard, Organometallics 16 (1997) 5857. (c) M.J. Scott, S.J. Lippard, Organometallics 17 (1998) 466. (d) M.J. Scott, S.J. Lippard, Organometallics 17 (1998) 1769. (e) K.J. Franz, S.J. Lippard, J. Am. Chem. Soc. 120 (1998) 9034.

[8] (a) R.D.W. Kemmitt, D.R. Russell, in: G. Wilkinson, F.G.A. Stone, E.W. Abel (Eds.), Comprehensive Organometallic Chemistry, vol. 5, Pergamon, Oxford, UK, 1982, p. 81. (b) J.M. Pratt, J.P. Craig, Adv. Organomet. Chem. 11 (1973) 331.

[9] (a) D. Mansuy, M. Lange, J.C. Chottard, J.F. Bartoli, B. Chevrier, R. Weiss, Angew. Chem. 90 (1978) 828. (b) D. Mansuy, Pure Appl. Chem. 52 (1980) 681. (c) L. Latos-Grazynski, R.-J. Cheng, G.N. La Mar, A.L. Balch, J. Am. Chem. Soc. 103 (1981) 4270. (d) A.L. Balch, R.-J. Cheng, G.N. La Mar, L. Latos-Grazynski, Inorg. Chem. 24 (1985) 2651. (e) P.J. Brothers, J.P. Collman, Acc. Chem. Res. 19 (1986) 209. (f) D. Mansuy, Pure Appl. Chem. 59 (1987) 759. (g) I. Artaud, N. Gregoire, J.-P. Battioni, D. Dupre, D. Mansuy, J. Am. Chem. Soc. 110 (1988) 8714. (h) I. Artaud, N. Gregoire, P. Leduc, D. Mansuy, J. Am. Chem. Soc. 112 (1990) 6899. (i) J.R. Wolf, C.G. Hamaker, J.-P. Djukic, T. Kodadek, L.K. Woo, J. Am. Chem. Soc. 117 (1995) 9194. (j) C.J. Ziegler, K.S. Suslick, J. Am. Chem. Soc. 118 (1996) 5306. (k) D. Mansuy, J.P. Mahy, in: F. Montanari, L. Casella (Eds.), Metalloporphyrins Catalyzed Oxidations, Kluwer, Dordrecht, The Netherlands, 1994, pp. 175–206.

[10] G. Wilkinson, R.D. Gillard, J.A. McCleverty (Eds.), Comprehensive Coordination Chemistry, (a) Ch. 45, and (b) Ch. 48, vol. 4, Pergamon, Oxford, UK, 1987.

[11] (a) M.C. Weiss, B. Bursten, S.M. Peng, V.L. Goedken, J. Am. Chem. Soc. 98 (1976) 8021. (b) M. Weiss, G. Gordon, V.L. Goedken, Inorg. Chem. 16 (1977) 305. (c) L.F. Warren, V.L. Goedken, J. Chem. Soc. Chem. Commun. (1978) 909. (d) G. Gordon, P.W. De Haven, M.C. Weiss, V.L. Goedken, J. Am. Chem. Soc. 100 (1978) 1003. (e) P.W. De Haven, V.L. Goedken, Inorg. Chem. 18 (1979) 827. (f) M. Tsutsui, R.L. Bobstein, G. Cash, R. Pettersen, Inorg. Chem. 18 (1979) 758. (g) V.L. Goedken, J.J. Pluth, S.M. Peng, B. Bursten, J. Am. Chem. Soc. 98 (1976) 8014. (h) V.L. Goedken, S.M. Peng, J.A. Molin-Norris, Y. Park, J. Am. Chem. Soc. 98 (1976) 8391. (i) M.C. Weiss, V.L. Goedken, Inorg. Chem. 18 (1979) 819. (j) V.L. Goedken, S.M.

Peng, Y. Park, J. Am. Chem. Soc. 96 (1974) 284. (k) V.L. Goedken, Y.A. Park, J. Chem. Soc. Chem. Commun. (1975) 214. (l) V.L. Goedken, S.M. Peng, J. Chem. Soc. Chem. Commun. (1975) 258. (m) P. Berno, C. Floriani, A. Chiesi-Villa, C. Guastini, J. Chem. Soc. Dalton. Trans. (1989) 551. (n) P. Berno, C. Floriani, A. Chiesi-Villa, C. Guastini, J. Chem. Soc. Dalton. Trans. (1988) 1409. (o) M.C. Weiss, V.L. Goedken, Inorg. Chem. 18 (1979) 819.

[12] (a) F.A. Cotton, J. Czuchajowska, Polyhedron 9 (1990) 2553. (b) F.A. Cotton, J. Czuchajowska, Polyhedron 9 (1990) 1221. (c) F.A. Cotton, J. Czuchajowska, J. Am. Chem. Soc. 113 (1991) 3427. (d) F.A. Cotton, J. Czuchajowska, X. Feng, Inorg. Chem. 29 (1990) 4329. (e) F.A. Cotton, J. Czuchajowska, L.R. Falvello, X. Feng, Inorg. Chim. Acta 172 (1990) 135.

[13] S. Ciurli, E.M. Meyer, C. Floriani, A. Chiesi-Villa, C. Guastini, J. Chem. Soc. Chem. Commun. (1987) 281.

[14] A. Klose, E. Solari, C. Floriani, N. Re, A. Chiesi-Villa, C. Rizzoli, Chem. Commun. (Cambridge) (1997) 2297.

[15] (a) G. Fachinetti, C. Floriani, F. Zanazzi, A.R. Zanzari, Inorg. Chem. 18 (1979) 3469. (b) S. Gambarotta, M. Mazzanti, C. Floriani, M. Zehnder, J. Chem. Soc. Chem. Commun. (1984) 1116. (c) S. Gambarotta, F. Urso, C. Floriani, A. Chiesi-Villa, C. Guastini, Inorg. Chem. 22 (1983) 3966.

[16] (a) T. Mashiko, C.A. Reed, K.J. Haller, W.R. Scheidt, Inorg. Chem. 23 (1984) 3192. (b) S. Ciurli, S. Gambarotta, C. Floriani, A. Chiesi-Villa, C. Guastini, Angew. Chem. Int. Ed. Engl. 25 (1986) 553. (c) G.S. Srivatsa, D.T. Sawyer, N.J. Boldt, D.F. Bocian, Inorg. Chem. 24 (1985) 2123.

[17] G.R. Eaton, S.S. Eaton, J. Am. Chem. Soc. 97 (1975) 235.

[18] (a) A. Tullberg, N.G. Vannerberg, Acta Chem. Scand. Ser. A 28 (1974) 551. (b) H.J. Buser, D. Schwarzenbach, W. Petter, A. Ludi, Inorg. Chem. 16 (1977) 2704.

[19] M. Pierrot, R. Kern, R. Weiss, Acta Crystallogr. 20 (1966) 425.

[20] P.T. Manoharan, W.C. Hamilton, Inorg. Chem. 2 (1963) 1043.

[21] (a) S.M. Peng, J.A. Ibers, J. Am. Chem. Soc. 98 (1976) 8032. (b) W.R. Scheidt, K.J. Haller, M. Fons, T. Mashiko, C.A. Reed, Biochemistry 20 (1981) 3653. (c) C. Caron, A. Mitschler, G. Riviere, L. Ricard, M. Schappacher, R. Weiss, J. Am. Chem. Soc. 101 (1979) 7401.

[22] (a) V.L. Goedken, S.-M. Peng, J. Chem. Soc., Chem. Commun. (1974) 914. (b) G.N. Schrauzer, J.H. Weber, T.M. Beckham, J. Am. Chem. Soc. 92 (1970) 7078. (c) G. Costa, G. Mestroni, G. Tauzher, J. Chem. Soc. Dalton Trans. (1972) 450.

[23] (a) G. Fachinetti, C. Floriani, P.F. Zanazzi, A.R. Zanzari, Inorg. Chem. 17 (1978) 3002. (b) C. Floriani, G. Fachinetti, Transition Met. Chem. 1 (1976) 50. (c) A. Croisy, D. Lexa, M. Momenteau, J.M. Saveant, Organometallics 4 (1985) 1574.

[24] D. Ramprasad, G.P. Pez, B.H. Toby, T.J. Markley, R.M. Pearlstein, J. Am. Chem. Soc. 117 (1995) 10694.

[25] (a) A. Behr, Carbon Dioxide Activation by Metal Complexes, VCH, Weinheim, Germany, 1988. (b) D.H. Gibson, Chem. Rev. 96 (1996) 2063.

[26] J.-P. Djukic, D.A. Smith, V.G. Young Jr., L.K. Woo, Organometallics 13 (1994) 3020.

[27] (a) P. Schwab, R.H. Grubbs, J.W. Ziller, J. Am. Chem. Soc. 118 (1996) 100. (b) S.J. Miller, H.E. Blackwell, R.H. Grubbs, J. Am. Chem. Soc. 118 (1996) 9606. (c) B. Mohr, D.M. Lynn, R.H. Grubbs, Organometallics 15 (1996) 4317. (d) R.H. Grubbs, S.J. Miller, G.C. Fu, Acc. Chem. Res. 28 (1995) 446. (e) S.T. Nguyen, R.H. Grubbs, J.W. Ziller, J. Am. Chem. Soc. 115 (1993) 9858. (f) M.A. Esteruelas, F.J. Lahoz, E. Oñate, L.A. Oro, B. Zeier, Organometallics 13 (1994) 4258. (g) A. Hafner, P.A. van der Schaaf, A. Mühlebach, Chimia 50 (1996) 131.

[28] C.G. Barraclough, R.L. Martin, S. Mitra, R.C. Sherwood, J. Chem. Phys. 53 (1970) 1643.

[29] P.W.D. Boyd, D.A. Buckingham, R.F. McMeeking, S. Mitra, Inorg. Chem. 18 (1979) 3585.

[30] (a) O. Kahn, Molecular Magnetism, VCH, New York, 1993. (b) R.L. Carlin, Magnetochemistry, Springer, Berlin, 1986. (c) C.J. O'Connor, Prog. Inorg. Chem. 29 (1982) 203.

[31] W.R. Scheidt, C.A. Reed, Chem. Rev. 81 (1981) 543.

[32] W.R. Scheidt, M. Gouterman, in: H.B. Gray, A.B.P. Lever (Eds.), Iron Porphyrins, Addison-Wesley, Reading, MA, 1982, p. 89.

[33] (a) E.V. Ivanov, Thesis, Institute of Technical Physics, Moscow, Russia, 1969. (b) V.V. Zelentsov, Sov. Sci. Rev. B Chem. 81 (1981) 543.

[34] H. Köppen, E.W. Müller, C.P. Köler, H. Spiering, E. Meissner, P. Gütlich, Chem. Phys. Lett. 91 (1982) 348.

[35] (a) V. Petrouleas, J.P. Tuchagues, Chem. Phys. Lett. 137 (1987) 21. (b) E. König, G. Ritter, J. Dengler, S.M. Nelson, Inorg. Chem. 26 (1987) 3582. (c) J.-A. Real, J. Zarembowitch, O. Kahn, X. Solans, Inorg. Chem. 26 (1987) 2939.

[36] (a) J.-A. Real, H. Bolvin, A. Bousseksou, A. Dvorkin, O. Kahn, F. Varret, J. Zarembowitch, J. Am. Chem. Soc. 114 (1992) 4650. (b) J.-A. Real, I. Castro, A. Bousseksou, M. Verdaguer, R. Burriel, M. Castro, J. Linares, F. Varret, Inorg. Chem. 36 (1997) 455.

[37] D.C. Figg, R.H. Herber, I. Felner, Inorg. Chem. 30 (1991) 2535.

[38] (a) V.V. Zelentsov, G.I. Lapouchkin, S.S. Sobolev, V.I. Shipilov, Dokl. Akad. Nauk. 289 (1986) 393. (b) N. Sasaki, T. Kambara, Phys. Rev. B 40 (1989) 2442.

[39] R.A. Earnshaw, E.A. King, L.F. Larkworthy, J. Chem. Soc. A (1959) 2459.

[40] K.D. Hodges, R.G. Woollmann, S.L. Kessel, D.N. Hendrickson, D.G. Van Derveer, E.K. Barefield, J. Am. Chem. Soc. 101 (1979) 906.

[41] F.V. Wells, S.W. McCann, H.H. Wickman, S.L. Kessel, D.N. Hendrickson, R.D. Feltham, Inorg. Chem. 21 (1982) 2306.

[42] (a) R. Hoffmann, W.N. Lipscomb, J. Chem. Phys. 36 (1962) 2179. (b) R. Hoffmann, J. Chem. Phys. 39 (1963) 1397.

[43] (a) K. Tatsumi, R. Hoffmann, Inorg. Chem. 20 (1981) 3771. (b) L. Giannini, E. Solari, S. De Angelis, T.R. Ward, C. Floriani, A. Chiesi-Villa, C. Rizzoli, J. Am. Chem. Soc. 117 (1995) 5801.

[44] K. Tatsumi, R. Hoffmann, J. Am. Chem. Soc. 103 (1981) 3328 and Refs. therein.

[45] P. Hofmann, Electronic structures of transition metal complexes, in: K.H. Dötz, H. Fischer, P. Hofmann, F.R. Kreissl, U. Schubert, K. Weiss (Eds.), Transition Metal Carbene Complexes, VCH, Weinheim, 1983, p. 113.

[46] (a) E.G. Jäger, Z. Chem. 4 (1964) 437. (b) E.G. Jäger, Z. Anorg. Allg. Chem. 364 (1969) 177.

[47] E.A. Boudreaux, L.N. Mulay, Theory and Applications of Molecular Paramagnetism, Wiley, New York, 1976, pp. 491–495.

[48] G.M. Sheldrick, SHELX-76, Program for crystal structure determination, University of Cambridge, Cambridge, UK, 1976.

[49] G.M. Sheldrick, SHELXL-93, Program for crystal structure refinement, University of Göttingen, Göttingen, Germany, 1993.